TRIBHUVAN UNIVERSITY
INSTITUTE OF ENGINEERING
PULCHOWK CAMPUS

THESIS NO: S001/075

Dynamic Analysis of Flexible Pavement Under Accelerated Vehicle Loading

By

Bijay Ban

A THESIS

SUBMITTED TO THE DEPARTMENT OF CIVIL ENGINEERING

IN PARTIAL FULFILLMENT OF THE REQUIREMENTS FOR THE

DEGREE OF MASTER OF SCIENCE IN STRUCTURAL ENGINEERING

DEPARTMENT OF CIVIL ENGINEERING

LALITPUR, NEPAL

SEPT, 2021

TRIBHUVAN UNIVERSITY
INSTITUTE OF ENGINEERING
PULCHOWK CAMPUS
DEPARTMENT OF CIVIL ENGINEERING

The undersigned certify that they have read, and recommended to the Institute of Engineering for acceptance, a thesis entitled "**Dynamic Analysis of Flexible Pavement Under Accelerated Vehicle Loading**" submitted by Bijay Ban (075/MSStE/001) has been supervised and recommeded to the Institute of Engineering for the partial fulfillment of requirement for the degree of Master of Science in Structural Engineering.

..……..……

Supervisor, Dr. Jagat Kumar Shrestha
Associate Professor
Department of Civil Engineering
Pulchowk Campus, Institute of Engineering

..……..……

External Examiner, Dr. Bijay Jaisi
Director
Quality, Research and Development Centre
Department of Road

..……..……

Committee Chairperson, Dr. Kamal Bahadur Thapa
M.Sc Co-ordinator
Department of Civil Engineering
Pulchowk Campus, Institute of Engineering

Date..……

COPYRIGHT

ABSTRACT

A three-dimensional flexible pavement simulated in ANSYS for typical road section in Nepal. The pavement's adopted finite element model (FE) is validated with the classical theoretical formulations for half-space pavement. The validated model is further utilized to understand pavement response with and without considering friction between the pavement and material nonlinearity. The material properties of pavement considered in the analysis is taken from typical road section used in Nepal. The inclusion of friction in FEM pavement represents more to the realistic nature of pavement with which the computation becomes more demanding due to frictional nonlinearity. The vertical displacement has increased while the stress and strain have decreased compared to the bonded model. The nonlinear pavement model produce response result always higher than the corresponding elastic loading under accelerated vehicular loading. The vertical displacement at bottom of asphalt is about 19 % and 12 % larger for nonlinear response. A comparison between maximum response during constant velocity and deaccelerated loading, the maximum stress on pavement under deaccelerated loading (with 5 m/s^2 from 10km/hr to 5 km/hr) is lesser than the constant velocity loading (5km/hr) while is greater than vehicle loading moving with 10 km/hr. The result of pavement from ANSYS simulation can be used for designing purpose basesd on iterative modeling of section for economical and safe design.

Keywords: Three-Dimensional Elastic Analysis, Dynamic Analysis, Flexible Pavement, Vehicular load, Accelerated effect

ACKNOWLEDGEMENT

I wish to express my sincere gratitude to my supervisor Asso. Prof. Dr. Jagat Kumar Shrestha, for his continuous guidance, inspiration, and encouragement during the thesis work and study period. I would like to thank Dr. Kshitij Charana Shrestha and Dr. Rojee Pradhananga for lectures and advices, proved to be valuable in the process of this thesis work.

I would like to express my great appreciation Asso. Prof. Dr. Kamal Thapa, our program coordinator for providing valuable guidance throughout the progress of this thesis work. I would also like to acknowledge all the faculty members of Department of Civil Engineering for the knowledge and concepts they gave me during my study at IOE, Pulchowk Campus.

I am thankful to Roads Board Nepal for providing financial supports to conduct this work. Also I am thankful to Centre of Infrastructure Development Studies (CIDS) for providing technical support and knowledge for completion of this study.

I would like to thank Er. Nishan Thapa, Er. Pramod Tiwari, Er. Sangita Acharya, Er. Prabin Wagle and my classmates for their direct and indirect help over the period of my master's study as well as this thesis.

To my family, thank you for encouraging me in all of my dreams and inspiring me during the thesis work.

I would like to recognize the assistance obtained through the reference books and research papers and would like to thank their authors.

Bijay Ban
075/MSStE/001
Sept 2021

TABLE OF CONTENTS

LIST OF TABLES

LIST OF FIGURES

LIST OF SYMBOLS

M = Mass stiffness matrix

C = Damping matrix

K = Stiffness matrix

$\ddot{u}$ = acceleration vector

$\dot{u}$ = velocity vector

u = Displacement vector

P = External force vector

α & β = Rayleigh damping coefficients

ω_i = Natural frequency of pavement system of mode i

ω_j= Natural frequency of pavement system of mode ii

ξ_i = Modal damping ratio of mode i

ξ_j = Modal damping ratio of mode j

ε = Stress tensor

G(t) = Shear relaxation function

K(t) = Bulk relaxation function

E = Strain tensor

T = Reduced relaxation time

I = Unit Tensor

M = Poisson ratio

αT = Time-temperature shift factor

C_1 & C_2 = Regression coefficients

T = Analysis temperature

T_{ref} = Reference temperature

LIST OF ACRONYMS AND ABBREVIATIONS

AASHTO = American Association of State Highway Transportation Officials

DOR = Department of Roads

FEM = Finite Element Modeling

3D = Three-dimensional

FEA = Finite Element Analysis

ANSYS = Analysis System (A FEM Software)

IRC = Indian Roads Congress

CHAPTER 1: INTRODUCTION

1.1 Introduction

The overall functioning of the highway system greatly relies on the performance of its pavements. The pavements design procedure determines pavement distress, life cycle, and overall functioning. Empirical methods, namely, American Association of State Highway Transportation Officials (AASHTO 1993) and Road Note 31 (1984), are followed to design flexible pavements worldwide. Department of Roads (DOR), Nepal has provided a guideline for the design of flexible pavements (DOR, 2014), which uses empirical method following the Indian Roads Congress IRC 37 guidelines (Koti Marg & Puram, 2018), American Association Of State Highway and Transportation Officials Guides for Design of Pavement Structures (AASHTO, 1993) and Road Note 31 (Road Note 31, 1984). In the guidelines of DOR, flexible pavements are designed as three-layered structures, and stresses and strains at critical locations are computed using the linear elastic model (DOR, 2014). However, as compared to the empirical design method used in DOR guidelines, the mechanistic-based design method can provide better insight for designing with the various combinations of material properties and its stress and strain nature in the pavement layers.

1.2 Problem Statement

One of the biggest problems in Nepal in the past is that the designed pavements are not lasting their intended service period for several reasons such as faulty constructional materials, improper supervision, etc. Among many other causes, the poor design methodology is also a significant cause. As DOR's (2014) suggestion, the design methodology for a country should be defined based on the local conditions, i.e., climatic, socio-economic, and technological development, and so on. However, there is a noticeable gap in research for the new design methodology in Nepal.

1.3 Objectives

The general objective of this thesis is to determine the response of flexible pavement under accelerated vehicular loading.

Specific Objective

- To analyze the response of vehicular load moving with different speeds on the pavement structure.

- To determine the effect of spatial distribution of load.
- To determine the effect of friction on the pavement interface
- To determine pavement response with the nonlinear material properties and understand the nature of the response to the linear material model.

1.4 Limitation of Research

The limation of the research are listed below

1. The vehicular loading is assumed to have uniform contact pressure and triangular loading variation on the magnitude.
2. The nonlinear material for pavement simulation is taken from the research paper, as the experiment is not performed to determine properties.
3. The horizontal component of vehicular loading is not considered.
4. Fatigue and rutting of the pavement are not included in the research.

1.5 Organization of Thesis

The whole research work has presented in eight chapters. Chapter 1 includes an introduction regarding why this thesis has been carried out. Chapter 2 outlines the literature review contains for this thesis and the research gap. The methodology followed in this thesis is presented in Chapter 3. Chapter 4 contains the procedure of how finite element modeling of pavement is performed in ANSYS. The linear finite element analysis of pavement is represented in chapter 5 and nonlinear finite element analysis in Chapter 6. The accelerated loading analysis of pavement is outlined in chapter 7. Based on the result and discussion from chapters 5-7, the conclusion drawn is presented in chapter 8 and recommendations for future works.

In this research, a three-dimensional (3D) finite element (F.E.) model of pavement is simulated in the ANSYS Mechanical APDL, with the validated F.E. model subjected to various loading parameters to understand the pavement's response. The developed F.E. model is capable of simulating the response of a flexible pavement subjected to vehicular loading. The model is applied for various pavements' composition/thickness under the loading to get insight into the effect of its structural response. The effect of acceleration loading could be significant for the flexible pavement section as in bridge entrant, zebra crossing, converging road section, start and end of speed limit pavement section, etc. The result of flexible pavement from modeling could be used for designing purposes based on iterative modeling of sections for economical and safe design. A

thorough discussion is made to understand the effect of vehicular motion with different velocities/accelerations on stresses and strains experienced by the pavement, particularly for Nepalese conditions, which have not been documented yet.

CHAPTER 2: LITERATURE REVIEW

Researchers have developed various models for the simulation of flexible pavement with various assumptions according to their purpose, accuracy, and efficiency required at the time. These models and methods range from a low level of complexity to very high levels of complexity. In the early 19's, flexible pavement responses and design are usually determined by using layers elastic theory such as proposed by Burmister (1945); Odemark (1949), considering elastic half-space under static loading. Analytical models of pavement structure of complex boundary with nonlinear properties are generally complex, and closed-form solutions may not be obtained.

With the development of high-speed computers, it has recently become able to handle complex boundaries, loading conditions, and nonlinear material properties. Lu & Wright (1998), in their research paper, simulated pavement using a two-dimensional 2D plane strain model to evaluate pavement performance. Also, Li et al. (2017) simulated 2D F.E. axisymmetric modeling. However, the three-dimensional simulations gave more reasonable results than the two-dimensional simulations when compared with actual measurements under traffic loading (Cho et al., 1996). Thus, more 3D FEM elements modeling is being created with the purpose of obtaining a more accurate response of the model to reality. Zaghloul et al. (1994) were among some of first, to develop a 3D model which is capable of capturing the response of moving load. Later the several 3D finite element models have been proposed by various researchers such as (Al-Qadi et al., 2008; Beskou, Hatzigeorgiou, et al., 2016; Beskou, Tsinopoulos, et al., 2016; Gungor et al., 2016; B. Huang et al., 2001)

Accurate modeling analysis of the pavement system also requires adopting an ideal constitutive model for each layer of pavement in simulation (Ali et al., 2009; M. Li et al., 2017). Researchers have used elastic material properties in modeling of pavement structure (Beskou & Theodorakopoulos, 2011). However, the use of elastic material properties underestimates pavement response by a lot compared to that of actual response(Beskou, Tsinopoulos, et al., 2016). Thus, the need of nonlinear material properties modeling has arisen. Researchers have been using nonlinear material properties of pavement to simulate the response of FEM closer to actual response under vehicular loading. Beskou, Hatzigeorgiou, et al. (2016); Cebon (1999); Chen (2009); González et al. (2007); C. W. Huang et al. (2011); Li et al. (2017); Saleeb et al. (2005). etc., have used viscoelastic and viscoplastic constitutive models in F.E. simulation.

The load exerted by vehicles on the pavement is non-uniform and depends on the tire construction, tire load, and tire inflation pressure (De Beer, 1996), resulting in complexity in modeling. So, for the simulation of vehicular loading, various loading simulations are considered according to their accuracy and convenience. Vehicular loading has been simulated as pulse rolling load (Lu & Wright, 1998), stationary transient loading (Howard & Warren, 2009), impulse loading (Ali et al., 2009; Cebon, 1999), dynamic loading by moving coordinate (Shen & Kirkner, 2001), transient local dynamic loading (Assogba et al., 2020; Yoo & Al-Qadi, 2007), etc.

The use of dynamic loading in the F.E. simulation results in a much closer response of nature under vehicular loading than static F.E. simulation using nonlinear properties (Beskou, Hatzigeorgiou, et al., 2016; B. Huang et al., 2001). Beskou & Theodorakopoulos (2011) have reported much more insight on the background on the case of nonlinearity and dynamic loading, in which they appleade for more research is needed towards the development and analysis of more realistic system models capable of exhibiting nonlinear behavior, including fatigue and permanent deformation features.

Table 2.1:.Summary of Literature Review

S.N	**Model Type**	**Material Behavior**	**Loading**	**Researchers**
1.	Analytical			
		Elastic	Static	Burmister, 1945 and Odemark, 1949
2.	FEM			
	2D plane strain	Non-Linear	Dynamic	Lu & Wright, 1998
	2D axisymmetric	Non-Linear	Dynamic FWD	Li et al., 2017
	3D model	Elastic, Linear	Static	Beskou & Theodorakopoulos, 2011
	3D model	Non-Linear	Dynamic	Beskou, et al., 2016; Assogba et al 2020

CHAPTER 3: METHODOLOGY

3.1 General

The research was conducted to determine the parameters influencing the response of the road pavement and their effects on the economic design of the pavement. The response of the pavement under various load cases varying the pavement material as per the need of the study was determined using finite element analysis. The finite element analysis for this research was performed on ANSYS Version 20 (a commonly available commercial finite element software). This research is highly motivated by the work done by (Beskou, Hatzigeorgiou, et al., 2016).

The methodology carried out in this research can be summarized in the steps as follows:

- A finite element modeling of the pavement structure was carried out in Finite Element Software ANSYS.
- Modeling of vehicle load
- Modeling of the material behavior of the pavement layers
- Analysis of model using the time-domain formulation
- The finite element model was validated with theoretical and researcher's works
- Thus, the model was analyzed for design load cases, and the results for various design parameters were compared.

The steps can be summarized in the flow chart as shown below:

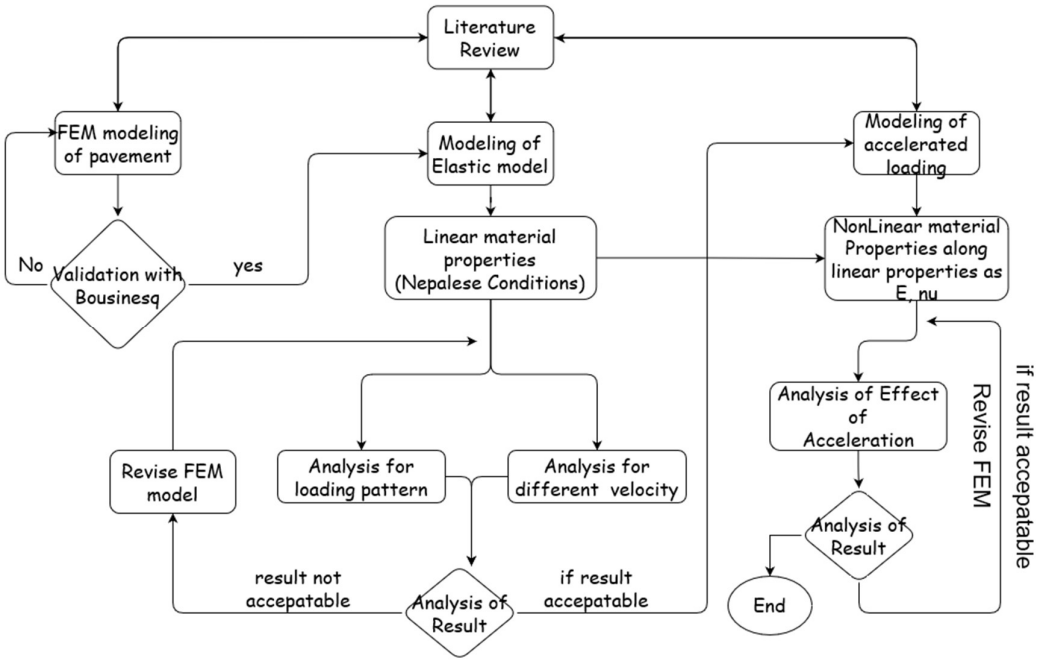

Figure 3.1:.Flowchart of Methodology.

3.2 Equation of Motion

A structure can be analyzed as static, quasi-static, and dynamic, each analysis method having its owns advantages and limitations. The types of analysis to be performed on the structure depend on the loading and natural frequency of the structure. Static analysis is generally performed for the body in which the acceleration of the body is zero or near about, i.e., where inertia force can be neglected. A structure subject to loading in which the acceleration of the body is significant is solved by dynamic analysis. It results in a more accurate solution than static analysis as inertial forces due to acceleration of the body are also considered. In Quasi-Static Analysis, we analyze the structure as being in static equilibrium at the given instant of time and consider inertial force as external loading at that time such that the summation of all forces in bodies is zero. This results in some approximation compared to dynamic analysis but significantly reduces computational time and are generally performed when inertia & damping effects are low. Equation of motion in matrix form for dynamic Analysis (Arros, 2002) of the pavement structure is shown in Equation (3.1).

$$[M]\{\ddot{u}\} + [C]\{\dot{u}\} + [K]\{u\} = F(t) \tag{3.1}$$

where [M], [C], and [K] are mass, damping, and stiffness matrices, respectively; $\{\ddot{u}\}$, $\{\dot{u}\}$, $\{u\}$ and {P} are acceleration, velocity, displacement and external force vectors. The pavement was initially considered to be in rest, i.e., initial displacement and velocity vector be to zeros.

The analytical solution of pavement's equation of motion under nonlinear material is complicated and cannot be determined for some load cases. Thus, Finite element analysis was carried out to determine the solution. The FEA of the dynamic equation of motion can be solved in the frequency domain by using the likes of the Fourier method or in the time domain by using direction integration methods such as implicit and explicit modes. The nonlinear dynamic analysis problems are commonly solved by using the direct integration method in the time domain. The analysis in this thesis was carried out using an implicit dynamic analysis procedure since it provides better numerical stability than explicit analysis and is generally efficient for the level of frequency loadings observed in pavement structures. The stability is unconditionally preserved for the implicit method, so only the accuracy requirement needs to be considered in the determination of time increment. The time step for implicit integration

analysis was taken $\frac{1}{20}T$, where $T = 2\pi \,/\, \omega_{co},\ \omega_{co} = 4\,\omega_u$ where $\omega_{co}\ and\ \omega_u$ were cutoff frequency and highest frequency contained in the loading, which was determined by Fourier analysis.

3.3 Material Damping

In dynamic analysis, it is required to determine the damping coefficient matrix of materials, which depends on structure, energy dissipation mechanism, viscosity, etc. of materials. The actual determination of the damping matrix is a complex task. Upon for the analysis purpose, it is approximated by various models. Here, the Rayleigh damping method was used for determining the damping matrix, which is linearly proportional to the mass and stiffness matrices Equation (3.2).

$$[C] = \alpha[M] + \beta[k] \tag{3.2}$$

where α and β are Rayleigh damping coefficient which is determined in terms of the natural frequencies of the pavement system ω_i and ω_j and corresponding modal damping ratio ξ_i and ξ_j. The modal damping ratios were considered equal for simplification in modeling; then, the damping coefficients were determined by Equations (3.3) and (3.4).

$$\alpha = 2\omega_i\omega_j\xi \,/\, \left(\omega_i + \omega_j\right) \tag{3.3}$$

$$\beta = 2\xi \,/\, \left(\omega_i + \omega_j\right) \tag{3.4}$$

The damping ratio of pavement structure generally lies between 0.02 and 0.05 of critical damping (Zhong et al. 2002; Alqadi et al. 2008). Subgrade to natural soil was considered as elastic material without any other energy dissipation sources. That of viscoelastic damping was considered negligible compared to nonlinear damping, so 5% of critical damping was used for the layers in Finite element simulation.

3.4 Material Behavior of Pavement Layers

Mechanistic empirical-based pavement design requires mathematical modeling of the material behavior of the pavement layer. The models will have many approximations to reality, as the behavior of any material is extremely complex and cannot be represented fully in a model. The approximations made depend on the purpose and the

required precision of the model predictions. The response of material can be commonly idealized into the following models for many materials used in engineering fields.

i. Elastic model

The Elastic model can be used to represent any engineering material provided strain (ε) in its are significantly small. Upon unloading, the body returns to its original position and does not depend on the rate of loading. Many analyses of finite element modeling of pavement are initially carried out consider material properties as elastic for its simplification in the calculation and helping to get insight before carrying out complex material model.

ii. Viscoelastic model

The viscoelasticity model is used to model the time-dependent response of the material. Linear viscoelasticity is formulated in terms of rheological models such as Maxwell, Kelvin, Voigt, etc.

iii. Plastic model

The material deformation is elastic up to some threshold limit, beyond which permanent deformation occurs, which is time-independent. The plasticity model is useful in describing permanent deformation which occurs in metals, soil, and other engineering materials.

iv. Viscoplastic model

The viscoplastic model is a combination of the viscoelastic and plastic models, in which plasticity deformation is rate-dependent. It is used in the study of metals at high temperatures, clay, concrete, etc.

For finite element simulation of the pavement, pavement layers from road base to natural soil were considered isotropic linear elastic. The Young's moduli, Poisson's ratio required for linear elastic modeling was be determined from the various test such as back-calculation after falling-weight deflectometer tests. The material behavior of asphalt concrete is not the only time or frequency-dependent but also temperature-dependent. Thus, the material behavior of asphalt concrete was modeled as viscoelastic material whose stiffness depends on time, temperature, and the frequency of the applied load (Gungor et al., 2016; S. Li et al., 2016)

A generalized Maxwell model was used to model the viscoelastic behavior of asphalt layers and to simulate the dynamic behavior. The hereditary integral formulation of an isotropic viscoelastic material stress function can be expressed as Equation (3.5) (DeSalva, Gabriel J., Swanson, 1985).

$$\sigma(t) = \int_0^t 2G(t-\tau)\frac{de}{dt}d\tau \; + \; t\int_0^t k(t-\tau)\frac{d\Delta}{d\tau}d\tau \qquad (3.5)$$

where G(t) and K(t) = shear and bulk relaxation function, e and trace tr[ε] = deviatoric and volumetric parts of strain tensor; t = reduced relaxation time; I = tensor unit. Prony-Dirichlet Series was used to represent the time dependency response of the asphalt concrete (DeSalva, Gabriel J., Swanson, 1985).

$$G(t) = G_\infty + \sum_{i=1}^{n} G_i . \exp\left(-t/\tau_i\right) \qquad (3.6)$$

$$K(t) = K_\infty + \sum_{i=1}^{n} K_i . \exp\left(-t/\tau_i\right) \qquad (3.7)$$

3

where G_i, G_∞ = material constants; τ_i = retardation time; t = reduced relaxation time. The shear and bulk moduli of asphalt concrete were be determined from the relaxation modulus E(t) using the following relationship:

$$G(t) = \frac{E(t)}{2(1+\mu)} \qquad (3.8)$$

$$K(t) = \frac{E(t)}{3(1\; -\; 3\mu)} \qquad (3.9)$$

3.5 Vehicular Loading

The actual representation of moving vehicle loading in the finite element model is complex. The wheel stress distribution is non-uniform and depends on various parameters such as tire pressure, pavement stiffness, the velocity of the vehicle, etc. For simulation of the moving vehicle, we considered the wheel stress distribution to be uniform and rectangular, resulting in simplification of the computation without much deviation from non-uniform wheel stress distribution (Assogba et al., 2020).

Horizontal contact pressure does not have a significant impact on the pavement response slightly away from the loading. The research was more focused on the general trend on stress-strain of pavement, so local effect around the loading location due to

horizontal contact pressure was neglected. Thus, the only vertical contact pressure of the tire was considered and assumed to be uniformly distributed over the rectangular area for simplification as modeling three-direction tire pavement contact forces resulted in complexity in simulation.

A load of vehicle moving was applied on the nodal basis of the wheel's location on the surface of the pavement. At time *t* when the wheel of the vehicle is in node *I*, the load of the vehicle was applied on the node *I* as the wheel move to node *j* at time *t+1,* the load of the node *I* was unloaded, and the vehicle load was applied on the node *I+1*.

Haversine variation of the load has been considered to simulated magnitude variation of vehicle loads on pavements (Y. H. Huang, 2004). As shown in Beskou, Tsinopoulos et al. (2016), the triangular moving load variation is very close to that of a haversine variation. The result obtained is very close to that obtained from haversine variation. So, triangular load variation was taken in the study as it's easier to model in the program. The load step was repeated for another node on which the vehicle moves in the pavement.

3.6 Boundary Condition

For the computation of the pavement response, it is required that the structure is sufficiently constrained to prevent rigid body movement. Pavement is a continuous structure, modeling it with any boundary condition results in some error in analysis. Researchers have used continuum elements in boundaries to replicate the continuum domain in analysis; also, absorbing boundaries have been used to minimize the boundary effect on the pavement responses. The Analysis from Beskou (Beskou et al., 2016) has shown that if a sufficiently large dimension of the model is considered and the boundary at relatively away from the point of interest location does not significantly affect the value of the responses of pavement. The dimension of the model was determined from various trials and errors as having large geometry provides a more accurate result as boundaries effect on its is minimize while it required high computational times due to large geometry. Therefore, the various trail was performed to obtain the balance between accuracy and computation time and the dimension was taken from model having reasonably accurate result with lesser computational times.

In this current finite element modeling, roller boundaries were used for analyzing pavement. Consider finite element model of pavement’s geometry and loading on the

pavement was symmetrical about Y direction, so only half of the pavement model and vehicle loading was considered on the modeling.

CHAPTER 4: FINITE ELEMENT MODELING:

4.1 General

A 3D F.E. model of pavement was simulated in ANSYS V20 with dimensions of 25. 8m x 11.5m x 35m is shown in Figure 4.1. The pavement generally consists of four layers; asphalt, base, subbase, and subgrade. The material properties of the base and subbase are nearly similar, so only three layers were considered for the current F.E. modeling of the pavement, as presented in Figure 4.1. Table 1 contains information about the thickness and material of the pavement layer used in the simulation.

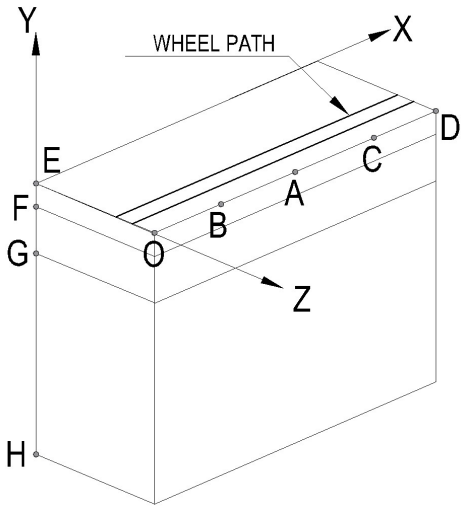

Figure 4.1:.A typical section of flexible pavement with pavement layers of asphalt-EF, base-FG and subgrade-GH.

4.2 Boundary Condition

The boundary condition and dimension considered in pavement structure play an important role in the analysis result. After completing several trials and mistakes to find a balance between accuracy and computing time, the model's dimensions were selected to be 25.8m x 11.5m x 35m. The vertical dimension has a significant effect on the accuracy of the result over other dimensions. Thus, a large dimension was considered in the vertical direction of the pavement model in the analysis as done by Assogba et al. (2020) and Beskou et al. (2016).

Vertical displacement at the bottom of the pavement was negligible considering large dimensions; therefore, the F.E. model was constrained in a vertical direction at the bottom of pavements. The lateral movement of pavement was constrained by applying roller on its lateral sides as pavement in nature is restrained in the lateral direction by its surrounding soil. The symmetrical vehicle loading and pavement geometry was considered during simulation. The roller boundary was applied on an axis of symmetricity, and the pavement was restrained sufficiently to prevent rigid body movement under loading.

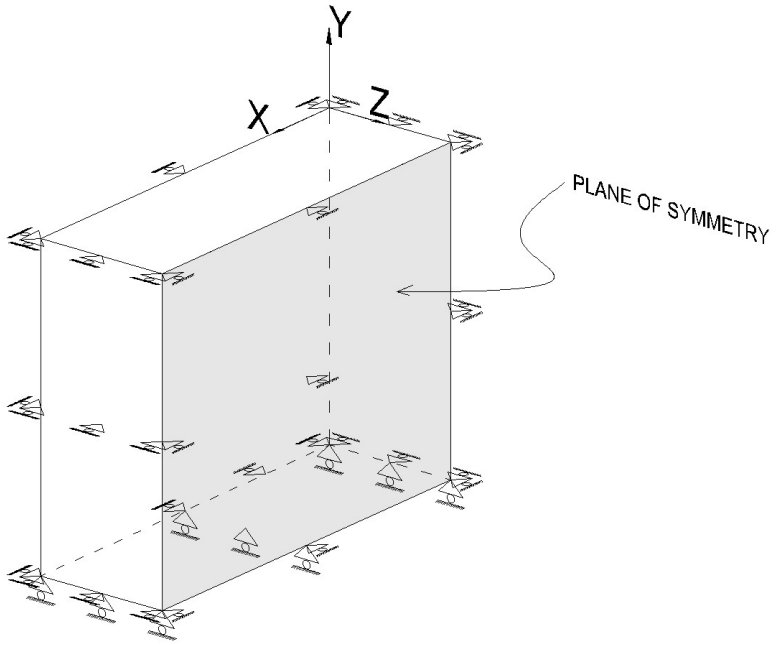

Figure 4.2:.Boundary Condition on Finite Element Modeling of Pavement

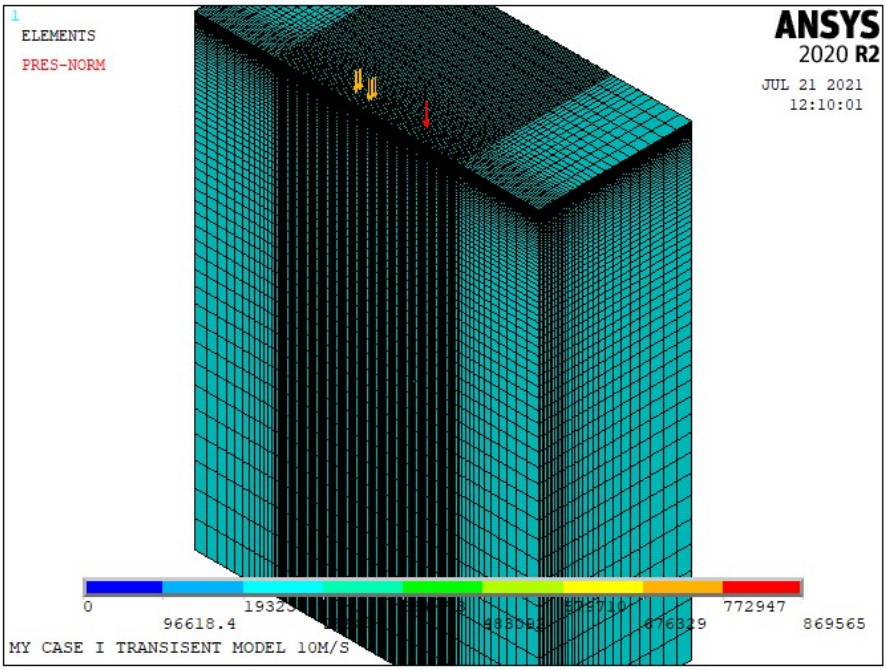

Figure 4.3:.Three-Dimensional finite element model of flexible pavement

4.3 Modeling of Vehicle and Loading Strategy

Tata motor (LPK 2518 6S 20 cum) shown in Figure 4.4 was taken as a representative vehicle to analyze vehicular loading responses on the pavement. It should be noted that this is a commonly available truck in Nepal, the dimension of which is shown in Table 4.1. For the design of pavement in Nepal, standard axle load is considered, so the analysis is also carried out for standard axle load, the specification of which is shown in Table 4.1

Table 4.1:.Vehicle specification (Tata-Motar, 2020)

Vehicle	LPK 2518,6s 20 cum
Wheel Base	4880 mm
Wight (Gross Vehicle Weight)	25000 Kg
Overall Length	8530 mm
Overall Width	2400 mm
Tire	10.00 x 20 – 16 PR
Inflation Pressure	109 psi

Figure 4.4:.Model vehicle representing commonly available truck in Nepal

The stress distribution is considered uniform and rectangular to simulate moving vehicles, resulting in computational simplification. In reality, the vehicle footprint is elliptical (Y. H. Huang, 2004), and contact stress on the pavement is coupled between tires and pavement. The elliptical tire footprint was converted into an equivalent rectangle area (Figure 4.5) of length and width $0.87L$ and $0.6L$, respectively, where L is the length of the elliptical footprint. The load on the wheel axle varies due to non-uniform load distribution on the steering and tandem axle resulting in the tire–pavement contact area varied from the one-wheel tire to another. For numerical modeling purposes and to simplify the APDL code, the tire-pavement contact stress was assumed to equal that of the tire's inflation pressure (Table 4.2), and the tire–pavement contact surface was assumed the same between all tires. For the Tata LPK vehicle, each tire footprint's equivalent length and breadth were 23 cm and 15 cm, respectively. The corresponding length and width of the DoR standard axle tire footprint were 32 cm and 22 cm, respectively, with uniform vertical contact stress of 0.57 MPa.

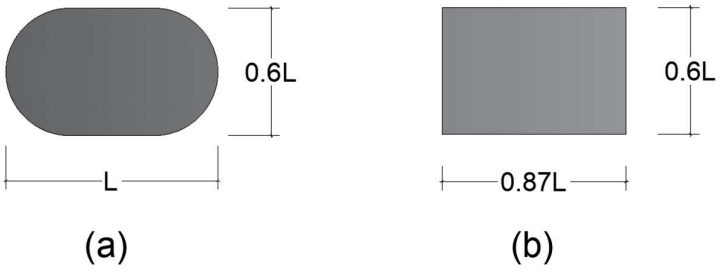

Figure 4.5:.(a) Elliptical footprint of tire (b) Equivalent rectangle footprint of tire; Area_equivalent = Area_elliptical = $0.52L^2$

Table 4.2:.Considered Truck LPK 2518, 6s 20 cum weight and tire contact area

Parameter	First-axle wheel	Tandem-axle wheel
Wheel configuration	Single	Dual
Gross Vehicle Wt. On axle (kN)	60	190
Inflation pressure (psi)	109	109
Tire pavement contact area (mm^2)	399	316
Length of elliptical footprint L (mm)	276	246
Length of equivalent area, 0.87L (mm)	240	214
Width of equivalent area, 0.6L (mm)	166	147

Table 4.3:.Considered single standard axle with the dual wheel of loading of 80 kN (DoR, 2021)

Parameter	Tandem-axle wheel
Wheel configuration	Dual
Load On axle (kN)	80
Load On dual wheel (kN)	40
Uniform vertical contact stress (MPa)	0.56
Tire pavement contact area (mm^2)	71428.57
Radius of circular contact area (mm^2)	150.8
Length of equivalent area, 0.87L (mm)	321.8
Width of equivalent area, 0.6L (mm)	221.9

The vertical contact pressure was only considered to simulate the dynamic effect of the pavement as the horizontal component does not found to have a significant impact on the general pavement response away from loading location according to the principle of Saint-Venant (1855). Further, modeling the three-directional tire–pavement contact forces is beyond the scope of this research.

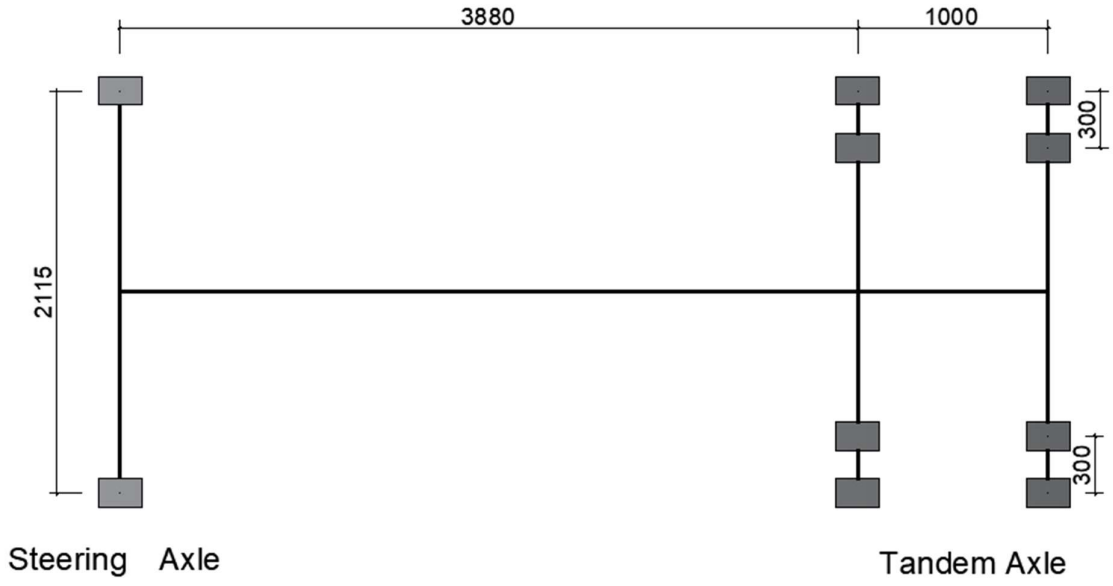

Figure 4.6:.Finite Element Modeling of Vehicle LPK 2518

4.4 Element Type & Size And Meshing

The pavement was model using SOLID185 (8-noded structural solid brick element). SOLID185 is available in two forms, a standard (non-layered) structural solid (KEYOPT (3) = 0) and a layered structural solid (KEYOPT (3) = 1) (DeSalva, Gabriel J., Swanson, 1985). The 2x2x2 integration point was taken to calculate stiffness, stress, and mass matrices, while the 2x2 integration point was taken for the pressure load vector. Figure 4.3 shows the generated F.E. model mesh. The model has meshed with a relatively finer mesh of element size of 0.115mm near the loading region and the area where high stress was developed. A relatively coarse mesh of average element size of 0.5 with their own bias in spacing along its layers was adopted elsewhere. A total of 2,29,840 elements was generated for this finite element modeling.

4.5 MATERIAL BEHAVIOR OF PAVEMENT LAYERS

4.5.1 Linear Material Behavior of Pavement Layers

The elastic material properties of the pavement layers are shown in Table 4.5 taken of commonly used value for road design in the Kathmandu valley as per AASHTO guideline. No interface element was modeled between pavement layers, and the layers are assumed to be perfectly bonded. For the preliminary understanding of the pavement response during the vehicle loading, a linear mathematical model is used before going to a nonlinear mathematical model. It helps in the intuitive understanding of the structure's response and provided valuable insight for nonlinear analysis.

Table 4.4:.Pavement Material Description

Pavement Layer	Material
Asphalt Surface Course	Modified Bitumen Surface Course
Asphalt Middle Course	DBM–I
Asphalt Bottom Course	DBM-II
Base Course	WMM
Sub-Base Course	GSB
Subgrade	Subgrade

Note: DBM – Dense bituminous macadam, WMM – Wet mix macadam, GSB –Granular sub base

Table 4.5:.Pavement Material Properties

Layers	Thickness (m)	Young Modulus (MPa)	Poisson Ratio	Density (kg/m^3)
Asphalt	0.19	2000	0.35	2500
Base	0.47	200	0.35	2667
Subgrade	34.33	62	0.35	1990

4.5.2 Nonlinear Material Behavior

The model using linear elastic constitutive relation results in simplification in the modeling and computation. However, the result from linear constitutive modeling is generally not in much agreement with reality nonlinear modeling, thus the need for nonlinear constitutive relation. The work from Beskou, Hatzigeorgiou, et al. (2016) has shown that pavement response with viscoelastic asphalt layer and elastic properties on

other layers exhibits similar dynamic behavior and response results to nonlinearity consider on base and subgrade layers. Thus the nonlinear pavement analysis is carried out by including nonlinearity in the asphalt layer only with the linear properties in other pavement layers. The asphalt layer of pavement was modeled as viscoelastic material as the material behavior of asphalt concrete is both time-dependent and temperature-dependent. Thus, the material behavior of asphalt concrete was modeled as viscoelastic material whose stiffness depends on time, temperature, and the frequency of the applied load (Li et al. 2015, Gungor et al., 2016). The hereditary integral formulation of the generalized Maxwell model (Equation 5) was used to express asphalt viscoelasticity, discussed in section 3.6. Table 4.6 contain material data of retardation time (τ_i) & shear relaxation modulus (G_i) need to define viscoelasticity for which four prony term was used. The value of material constant (G_i) is taken from the experimental results of Berthelot et al. (2003), which is scaled from *G(0)* = 817 MPa (Asphalt Specimen 900901) to *G(0)* =2000/2*(1+0.35) = 740.7 MPa to be compatible with the elastic properties of the asphalt layer, is shown in Figure 4.7.

Table 4.6:.Prony-Dirichlet Series for generalized Maxwell Model

No.	τ_i(s)	G_i(MPa)
1	20.0	3.92×10^1
2	2.0	1.23×10^2
3	1.0	1.19×10^1
4	0.2	3.04×10^2
∞	-	2.59×10^2

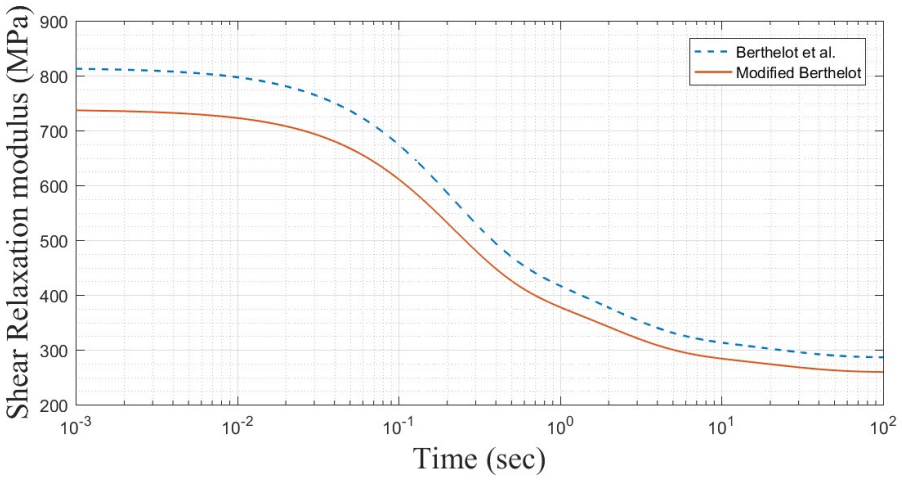

Figure 4.7:.Shear relaxation modulus of asphalt material

CHAPTER 5: LINEAR FINITE ELEMENT ANALYSIS

5.1 General

The pavement model produced in the preceding chapter must be validated before analyzing for various load scenarios with desired material characteristics. The model was verified to ensure that the method was followed and that the results were accurate. The validated model gave assurance that the model's results are accurate enough for future testing of varied loads and material characteristics.

5.2 Validation of the F.E. model

Validation of the modeling, it's meshing, boundary conditions, geometry loading, and the solution is conducted by comparing the result of the developed model to that of the theoretical value (Boussinesq, 1885). For the elastic half-space, the theoretical value for the vertical displacement and stresses along the x, y, and z-axis of the pavement under the distributed load, *p*, acting on the circular area of radius α on the surface of the pavement at a depth, *z*, can be determined by Equation (5.1, (5.2 and (5.3 (Boussinesq, 1885).

$$u_y = \frac{(1+v)p\alpha}{E} + \left[\left(1+\left(\frac{z}{\alpha}\right)^2\right)^{-0.5} + (1-2v)\left(1+\left(\frac{z}{\alpha}\right)^2\right)^{-0.5} - \left(\frac{z}{\alpha}\right)\right] \tag{5.1}$$

$$\sigma_y = p\left[1-\left(1+\left(\frac{\alpha}{z}\right)^2\right)^{-1.5}\right] \tag{5.2}$$

$$\sigma_x = \sigma_z = p\left[\frac{(1+2v)}{2} - (1+v)\left(1+\left(\frac{\alpha}{z}\right)^2\right)^{-0.5} + 0.5\left(1+\left(\frac{\alpha}{z}\right)^2\right)^{-1.5}\right] \tag{5.3}$$

where Young's modulus of elasticity, *E* is 50 x 10^6 N/m^2, Poisson's ratio, ν is 0.25 for all three layers. The load of the vehicle is applied as stationary distributed pressure acting on a rectangular area of 0.46m x 0.3m symmetrical about x-z around surface

point A of pavement, shown in Figure 4.2. The result of the numerical model is compared to that of the theoretical value determined by using Equation (5.1, (5.2, and (5.3 (Boussinesq, 1885), where α is the radius of a circle. The discrepancy between the numerical model and that of theoretical value is about 1-4 %, shown in Table 5.1. Understandably, the error in displacement is relatively lower than that of stresses since displacement is the primary result quantity obtained directly solving equilibrium equation. On the other hand, stresses are derived result quantities determined by using primary quantity resulting in some finite element errors. The normal stresses about *x* and *z* are slightly different, possibly due to unsymmetrical rectangle loading on the surface.

Table 5.1:.Response of uniform half-space pavement at z = -1.0 m due to vertically distributed pressure acting on a rectangular area of 0.46m x 0.15m on the surface of the pavement.

Parameter	Analytical	Numerical	Error
u_y	1.9390E-05	-1.90E-05	2.199%
σ_y	36284.92527	-35228	2.913%
σ_x	-1477.097878	1456.9	1.367%
σ_z	-1477.097878	1537.8	-4.110%

Table 5.2:.Material considered for comparison with IITPAVE Analysis

Effective CBR	7%
Thickness of Bituminous layer	190 mm
Thickness of granular base (WMM)	250 mm
Thickness of granular sub-base (GSB)	230 mm
Modulus of Bituminous layers	3000 MPa
Modulus of Base	200 MPa
Modulus of Subgrade	62 MPa
Poisson Ratio of Bituminous Layer	0.35
Poisson Ratio of Base	0.35
Poisson Ratio of Subgrade	0.35
Cumulative number of standard axles design	300 MSA

Table 5.3:.Response of pavement under standard axle load

	IITPAVE	FEM Model	Error
Horizontal tensile strain at bottom of bituminous layer (x 10^{-6})	146	130.60	10%
vertical compression strain at top of subgrade (x10^{-6})	243	233.2	4%

The response of pavement under standard axle load is determined for the material in Table 5.3. The response of pavement is determined using a 3D FEM model and compared to the IITPAVE result. The difference in the horizontal tensile strain at the bottom of the bituminous layer is only about 4 %. In comparison, there is a 13 % difference in vertical compression strain at the top of the subgrade between the two models due to more simplification of circular to rectangular for analysis. The strain range is acceptable compared to the IIPAVE result; therefore, this model is used for further investigation. The horizontal tensile stress (σ_z) at bottom of bituminous layer and vertical compression stress (σ_y) at the top of subgrade are 438 kN and 0.015.066 kN respectively.

5.3 Damping in Pavement

The modal analysis of pavement is carried out to determine the natural frequencies and estimate the damping characteristics of the pavement for dynamic analysis. Table 5.4 lists the natural frequencies of the pavement for the first five modes.

Table 5.4:.Natural frequency of pavement

Mode	Frequency (rad/sec)
1	1.5901
2	2.3276
3	3.2353
4	4.4154
5	4.576

For the computation of damping matrix $[C]$, the damping of the pavement is assumed to be of Rayleigh damping such that

$$[C] = \alpha_d[M] + \beta_d[K] \tag{5.4}$$

where α_d& β_d are the mass and stiffness damping coefficient. Assuming modal damping ratio corresponding to the natural frequency ω_i& ω_j of mode i and j of the pavement to be equal i.e $\xi_i = \xi_j = \xi$; the mass and stiffness damping coefficient can be determined using Equations (5.5) and (5.6) (Bathe K J., 2005).

$$\alpha_d = \frac{2\omega_i\omega_j}{\omega_i + \omega_j} \tag{5.5}$$

$$\beta_d = \frac{2\xi}{\omega_i + \omega_j} \tag{5.6}$$

The damping ratio is required to compute the mass and stiffness damping coefficient, which depends on the frequency of the structure. The damping ratio is assumed to be constant in the critical frequency range for simplicity; thus, the damping coefficients have the same critical damping ratio in the desired frequency range of the analysis. The pavement structure's first natural frequency and dominant loading frequency is taken as frequency range to determine the damping ratio, which is assumed constant in that range. The mass and stiffness coefficient of Rayleigh damping is determined to be 0.1558 and 0.0145 using Equation (5.5) and (5.6) where, $\omega_i$and ω_j are frequency for the constant Rayleigh damping in that range for which average of the first three natural mode frequencies and last two among the first five natural mode frequencies is considered. Experimentally the damping ratio (ξ) of the pavement is founded out to be in the range of 2 -5 % (Zhong et al 2002; Alqadi et al. 2008). In this study, the damping ratio (ξ) is taken to be 5% in all layers.

-5.4 Analysis of commercial vehicle (LPK)

The Tata vehicle (LPK 2518 6S 20) was modeled and analyzed on the F.E. pavement to investigate the effects of various speeds and anticipated load distributions on the LPK vehicle's wheels.

5.4.1 Effect of a different distribution of load on the Pavement

A case study is conducted to investigate the effect of the variable distribution of load on the pavement for which the vehicular load on the pavement is modeling in three different ways: i) series of distributed pressure (Case I) ii) series of concentrated forces (Case II), and iii) a point concentrated force (Case III) each having same resultant force of 250 KN. The response of the pavement under these different spatial vehicle load cases is shown in Table 5.5. It can be observed from Table 5.5 that the response of the pavement under the concentrated load is higher than under series of distributed pressure loads and concentrated load; however, the variation between them is not much. For the simplicity of modeling, a concentrated load can be used in the analysis without much effect on the result of the analysis.

Table 5.5:.Effect of different distribution of load on response of pavement

Case	*y(m)*	u_y *(mm)*	σ_y *(kPa)*	σ_x *(kPa)*	σ_z *(kPa)*	ε_y *(x 10^{-6})*	ε_x *(x 10^{6})*	ε_z *(x 10^{6})*
I	O (0.0)	-1.006	-152.8	-376.6	-370.4	-97.64	-96.72	-4.782
	EF (0.19)	-1	-109.4	-65.03	-5.579	-97.64	-1.558	-238.4
	FG (0.67)	-0.905	-23.5	-7.014	-0.417	-45.14	3.62E-05	-267.4
II	O (0.0)	-1.133	-1262	-427.5	-512	-67.11	-217.8	-504.9
	EF (0.19)	-1.029	-236.3	-87.81	-4.634	-67.11	-1.502	-457.1
	FG (0.67)	-0.893	-24.99	-6.943	-0.430	-44.96	3.559E-05	-289.7
III	O (0.0)	-1.544	-2520	-888.8	-961	-156.7	-377.6	-1010
	EF (0.19)	-1.336	-471.2	-99	-5.394	-156.7	-2.378	-921.7
	FG (0.67)	-1.019	-40.99	-7.99	-0.459	-51.04	3.49E-05	-501.8

Note: u_y – vertical displacement; σ_y, σ_x, and σ_z – *stress along y,x, and z-axis, respectively;* ε_y, ε_x, *and* ε_z – *strain along y,x, and z-axis respectively*

5.4.2 Response Analysis for static vehicular load

Table 5.6 shows the response of the pavement under static vehicular loading at the asphalt-base interface (point A) and base-subgrade interface (point B). With increasing depth, the response (displacement, stress, and strain) of pavement under vehicle load decreases. Table 5.6 illustrates a 14 percent reduction in vertical pavement displacement with a depth increase from 0.19m (point A) to 0.67m (point B) from the

surface. From point A to point B, there is an average 88 percent reduction in strain. whereas the vertical strain is reduced by 8 percent.

Table 5.6:.Static Response of Pavement under LPK 2518 vehicle load

y (m)	u_y (mm)	σ_y (kPa)	σ_x (kPa)	σ_z (kPa)	ε_y ($x10^6$)	ε_x ($x\ 10^6$)	ε_z ($x10^6$)
O (y =0.0)	-0.9226	-253.6	-472.8	-425.9	30.48	-117.5	-85.84
A(y=0.19m)	-0.9065	-135.8	126	92.2	-292.4	-117.5	100.5
B(y =0.67m)	-0.776	-23.53	9.512	10.05	-269.1	109.1	114.6

5.4.3 Response Analysis for various vehicle speed

To understand the influence of vehicle speed on pavement response, the FEM model is used to calculate the responses of an LPK vehicle (Figure 4.6) traveling on the surface of the pavement at various speeds.

Vertical Displacement (u_y) of Pavement

The time history of vertical displacement at critical points A and B is shown in Figure 5.1. The displacement of pavement is in direction of pressure and with the increase in depth, the displacement decreases. The two peaks observed on the curve during vehicle motion are due to the tandem wheel configuration of the vehicle. Each peak in the time history curve occurs when the vehicle wheel is at or just after passing the critical point. For obvious reasons, the increase in vehicle speed resulted in the earlier appearance of peak displacement in the pavement. However, with the increase in the vehicle speed, the magnitude of displacement decreases. This is understandably due to the reduction of contact time of vehicle and pavement with the increment in speed of the vehicle.

Table 5.7: Response of Pavement under Vehicle loading moving with different speed

v (m/s)	y (m)	u_y (mm)	σ_y (kPa)	σ_x (kPa)	σ_z (kPa)	ε_y ($x10^6$)	ε_x ($x\ 10^6$)	ε_z ($x10^6$)
5	O (0.0)	-1.027	-188.5	-424.2	-398.5	-108.6	-100.5	-4.52
	EF (0.19)	-1.018	-121.8	-74.65	-5.032	-108.6	-1.543	-256.8
	FG (0.67)	-0.9143	-23.67	-6.071	-0.2637	-38.06	2.1E-03	-269.9
10	O (0.0)	-1.006	-152.8	-376.6	-370.4	-97.64	-96.72	-4.782

	EF (0.19)	-1	-109.4	-65.03	-5.579	-97.64	-1.558	-238.4
	FG (0.67)	-0.9052	-23.5	-7.014	-0.4167	-45.14	3.618E-05	-267.4
20	O (0.0)	-0.9977	-109.4	-302.7	-329.6	-74.51	-93.35	-2.295
	EF (0.19)	-0.978	-91.52	-44.2	-4.656	-74.51	-1.73	-198.1
	FG (0.67)	-0.8767	-23.15	-6.929	-0.3545	-45.04	6.7E-03	-262.7
30	O (0.0)	-0.9239	-89.02	-267.2	-305.7	-64.71	-91.1	-1.282
	EF (0.19)	-0.9051	-82.47	-36.3	-5.409	-64.71	-1.658	-176.1
	FG (0.67)	-0.8084	-22.67	-6.868	-0.2535	-44.27	6.7E-03	-257.5

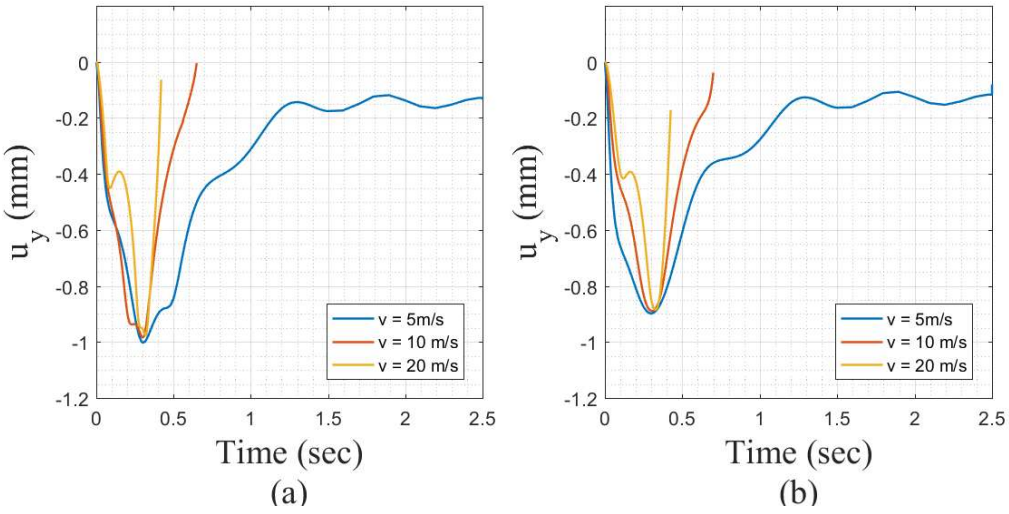

Figure 5.1:.Vertical displacement u_y time history at (a) point A (Asphalt-Base Interface) (b) Point B (Base-Subgrade Interface)

Stresses on Pavement

The time history curve for vertical stress (σ_y) at point A 190 mm from the top face and at point B 670 mm from the top face is presented in Figure 5.2. There is on average 90 % decrease in vertical stress from point A to point B. Further, Table 5.7 shows that with the increase in the velocity the magnitude of vertical stresses in the pavement layers goes on decreasing. The rate of decrease is more significant at the upper layers of the pavement and the effect is negligible at higher depths. As shown in Figure 5.2 and Table 5.7, the reduction in the magnitude of vertical stress at point A is 25 % for speeds of 20 m/s and 5 m/s and the same at point B was only 4 %. It can be observed that the two peaks also occur on the stress's time history. The vertical stress (σ_y) on base-asphalt and

subgrade–base interface is always on compression during the entire motion of the vehicle as shown in Figure 5.2. The stress variation is cyclic and the cycle of variation in stress occurs faster with an increase in velocity of the vehicle. The cyclic nature of stress goes on vanishing with an increase in the depth of the pavement. The lateral stresses along x are in both tension and compression near the surface at point A; however, with the increase in the depth nature of lateral stresses becomes tension.

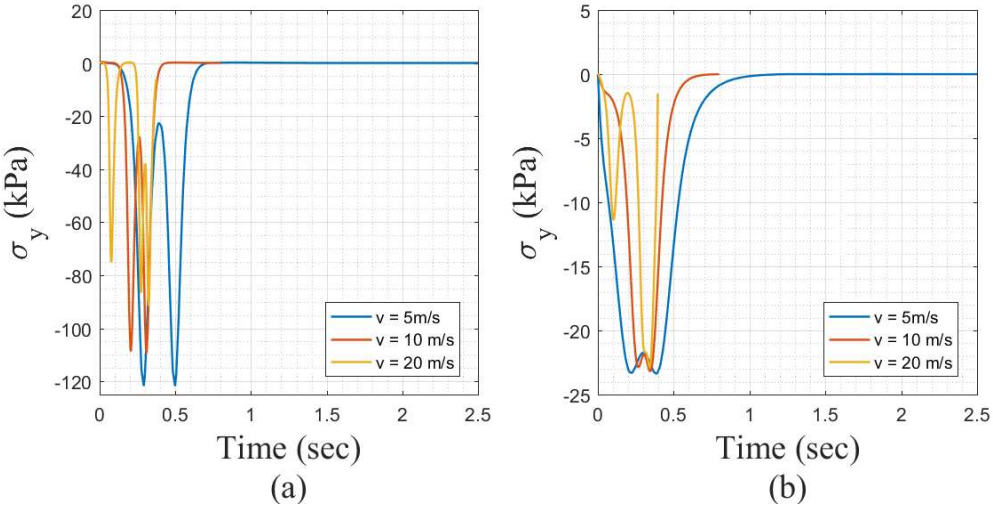

Figure 5.2:.Vertical stress σ_y time history at (a) Point A (Asphalt-Base Interaction) (b)Point B (Base-Subgrade Interaction)

Strains on Pavement

The time history curve for vertical strain (ε_y) at point B 670 mm from the top face is presented in Figure 5.3. Figure 5.3 also shows lateral strain (ε_z) at the pavement layer interface point A 190 mm from the top face. There is in average 47% decrease in vertical strain from point A to point B. Table 5.7 shows that with the increase in the velocity, the magnitude of vertical stresses in the pavement layers goes on decreasing. The rate of decrease is more significant at the upper layers of the pavement, and the effect is negligible at higher depths. As shown in Figure 5.3 and Table 5.7, the reduction in the magnitude of vertical stress at point A is 31% for speeds of 20 m/s and 5 m/s, and the same at point B was a 15% increment. Here also, it can be observed that the two peaks also occur on the stresses time history due to tandem wheel configuration. The vertical strain (ε_y) on base-asphalt and subgrade–base interface is always on compression during the entire motion of the vehicle as shown in Figure 5.3.

As in the stress, strain variation is also cyclic and the cycle of variation in stress occurs faster with an increase in velocity of the vehicle. The cyclic nature of strain goes on vanishing with the increase in depth of the pavement. The lateral strain along the z-axis is in tension along with depth as shown in Figure 5.3, There is an average of 93 % decrease in strain ε_z respectively from point A to point B. Further, Table 5.7 shows that with the increase in the velocity the magnitude of tensile strains in the pavement layers goes on decreasing. The rate of decrease is more significant at the upper layers of the pavement and the effect is negligible at higher depths. The reduction in the magnitude of stress (ε_z) at point A is 7%, for speeds of 20 m/s and 5 m/s respectively as shown in Figure 5.3.

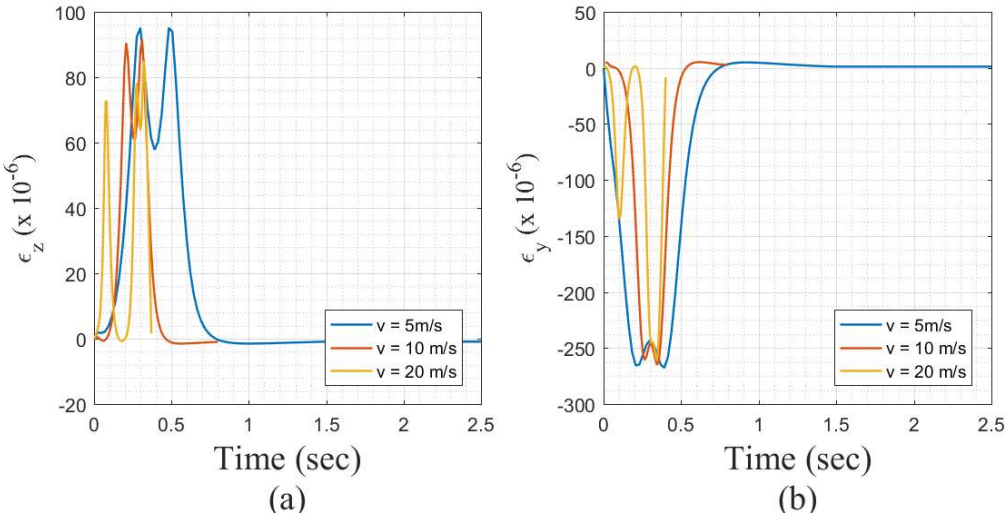

Figure 5.3:.(a) Lateral Strain ε_z at Point A (Asphalt-Base Interaction) and (b) Vertical Strain ε_y at Point B (Base-Subgrade Interaction)

5.4.3 Comparison of the response of pavement

The F.E. pavement is analyzed to a stationary and moving vehicle load at different speeds, and the maximum responses are shown in Table 5.6 and Table 5.7. The vertical response of pavement under moving vehicle load (displacement, stress, and strain) is larger than that of stationary vehicle load, whereas the lateral response is lower. For a stationary vehicle load and a moving load traveling at 5 m/s, there is an 11 percent increase in vertical displacement (u_y) and a 25 percent decrease in vertical stress (σ_y).

5.5 Analysis of pavement under standard axle load

The design of the pavement section in Nepal is carried out for the vehicular load in terms of standard axle wheel. So analysis is also carried out for the standard wheel load as in the previous section a commercial vehicle is considered.

5.5.1. Static response analysis

The static response of the pavement is performed, and maximum response at the bottom of the bituminous layers (A) and the top of the subgrade (B), is presented in Table 5.8. As in LPK vehicle, along the depth, the response of pavement decrease. The vertical displacement on point B from point A has decreased by 24 percent, while the stress and strain responses have decreased by 92 percent and 25 percent, respectively. The static response of bonded pavement determined in ANSYS simulation is shown in Figure 5.4, Figure 5.5, and Figure 5.6.

Table 5.8:.StaticResponse of Pavement under Vehicular load

y(m)	u_y *(mm)*	σ_y *(kPa)*	σ_x *(KPa)*	σ_z *(KPa)*	ε_y *(x 10^6)*	ε_x *(x 10^6)*	ε_z *(x 10^6)*
A(y=0.19)	-0.4938	-163	131.1	158.7	-338.4	134.1	104.3
B(y=0.67)	-0.3676	-17.26	10.86	9.274	-211	104.3	88

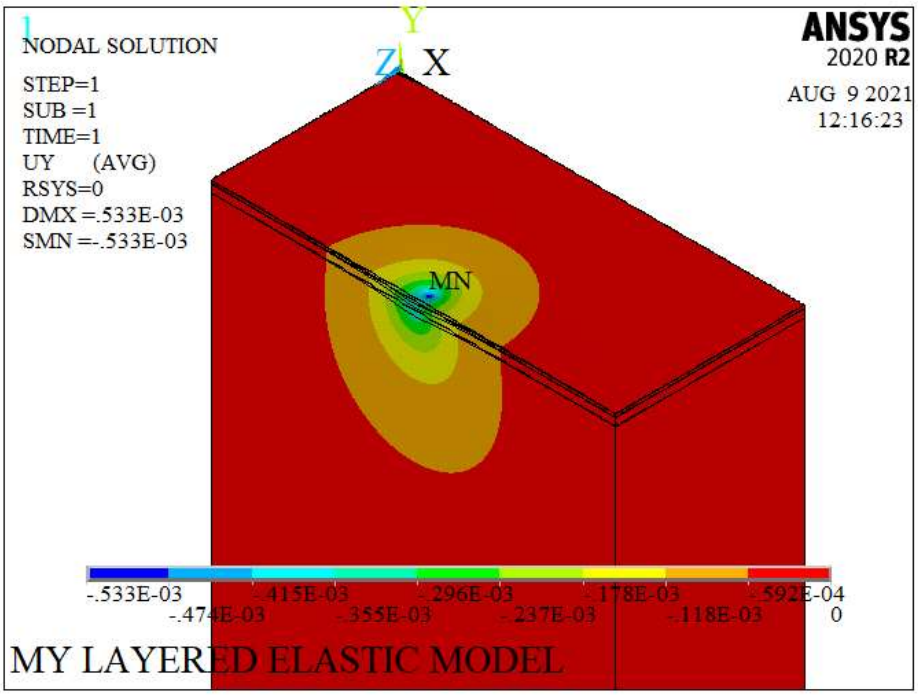

Figure 5.4:.Vertical Displacement (u_y) contour on the bonded pavement under static loading

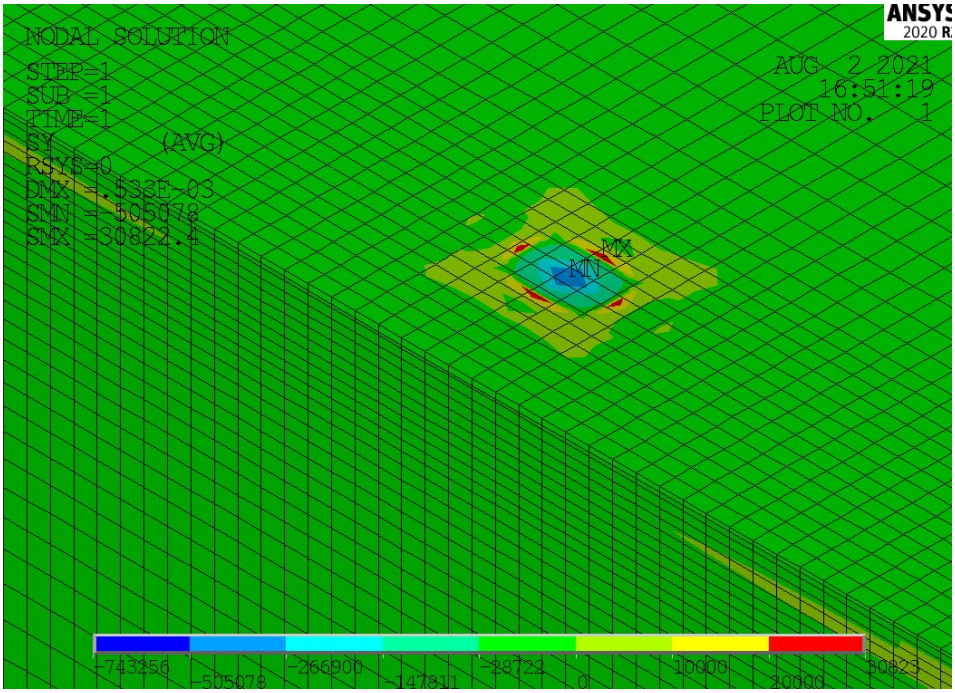

Figure 5.5:.Vertical Stress (σ_y) contour on the bonded pavement under static loading

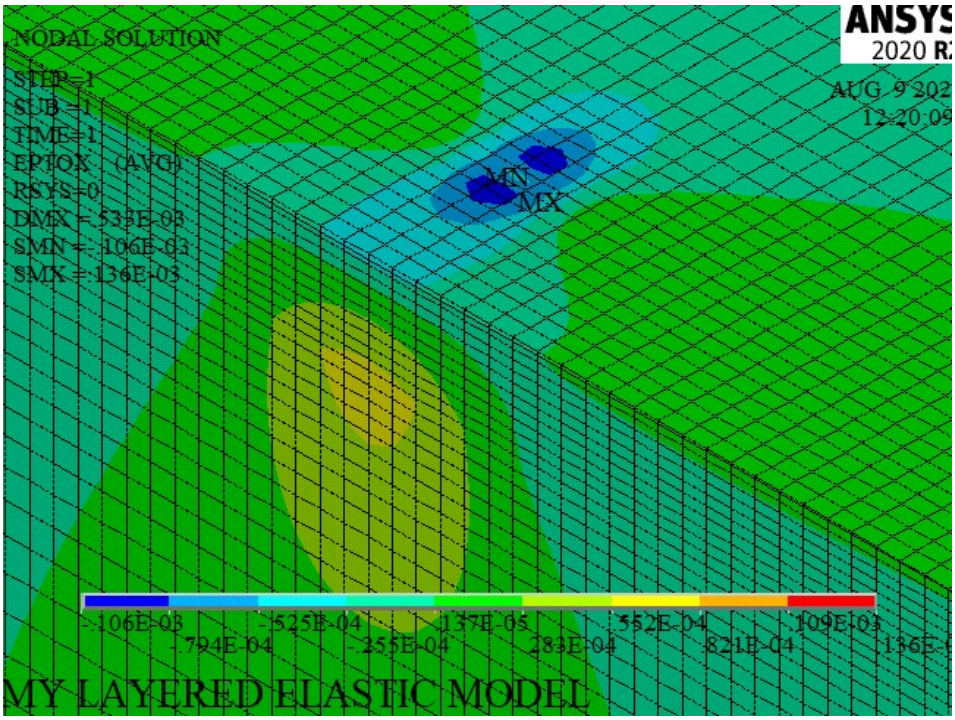

Figure 5.6:.Lateral Strain (ε_z) contour on bonded pavement under static loading

5.5.1 Response analysis under different vehicular speed

The analysis of pavement is performed for standard axle load moving with different speeds and presented in Table 5.9. One can observe from Table 5.9 the response of pavement decrease with an increase in velocity of axle load moving on the surface of the pavement. Increment of the velocity of axle load, The magnitude of vertical displacement at the bottom of bituminous layers is decreased by 0.677 % for an increase of velocity of 15 km/hr from 5 km/hr and 0.211% decrease at the top of subgrade, and the nature of vertical displacement is compressive in both location. The horizontal stress and strain are tensile at the top of the subgrade, while a small compressive strain occurs in the wheel load direction at the bottom of the asphalt layer. There is a decrease of 2.8% and 1.847% in magnitude at points A and B of vertical stress and strain on an increment of 10 km/hr from the initial velocity of 5 km/hr of vehicle.

Table 5.9:.Response of pavement under standard axle load moving with different velocity

Velocity (km/hr)	*y(m)*	*u_y (mm)*	*σ_y (kPa)*	ε_y *(x10⁶)*	ε_x *(x 10⁶)*	ε_z *(x 10⁶)*
5	A(y= 0.19)	-0.4612	-68.57		-23.63	

	B(y=0.67)	-0.3801	-13.64	-225.2	67.76	21.72
10	A(y= 0.19)	-0.4589	-66.74		-23.29	
	B(y=0.67)	-0.3799	-13.51	-222.9	64.59	21.65
15	A(y= 0.19)	-0.4581	-65.8		-22.56	
	B(y=0.67)	-0.3793	-13.47	-220.9	61.1	21.28
20	A(y= 0.19)	-0.4569	-65.91		-22.78	
	B(y=0.67)	-0.3785	-13.47	-222.9	61.91	21.33

CHAPTER 6: NONLINEAR FINITE ELEMENT ANALYSIS

6.1 General

The pavement was modeled with linear elastic material characteristics and the bonded interface between pavement layers in Chapter 5. In this chapter, pavement analysis is carried out by integrating nonlinear material characteristics and friction between pavement layers in pavement FE simulation, which is more realistically representable pavement. The difference in response is calculated to determine the difference in the result of not including nonlinearity.

6.2 Response of pavement considering friction

Pavement is a layered structure with a frictional interface between layers, so the study of the friction effect is carried out. The pavement's reaction to static and dynamic loads with the addition of friction is determined.

6.2.1 Static analysis

Table 6.1 contains the response of pavement under static standard wheel axle load at the pavement interface (i.e., asphalt-base and base-subgrade) with frictional nonlinearity interface between layers. When comparing with the linear static response (Table 5.3 and Table 6.1), it can be seen that the frictional pavement layer model has a 42 percent increase in vertical displacement (u_y) and a 20 percent increase in vertical stress (σ_y) when compared to the bonded model. In the case of lateral stress-strain, the frictional model increases by 74% and 37%, respectively. The discontinuities in the contour plot of response (displacement, stress, strain) in the frictional model, shown in Figure 6.1, Figure 6.2, and Figure 6.3, are caused by frictional resistance, which causes discontinuities in the response of pavement layers as layers are permitted to slide against one another

Table 6.1:.Static Response of frictional Pavement model under Vehicular load

y(m)	u_y *(mm)*	σ_y *(kPa)*	σ_x *(kPa)*	σ_z *(kPa)*	ε_y *(x 10^6)*	ε_x *(x 10^6)*	ε_z *(x 10^6)*
A(y=0.19m)	-0.8532	-232.6	555.5	612.5	-320.7	211.3	169.2
B(y=0.67m)	-0.5945	-19.17	38.87	33.58	-222.6	169.2	133.4

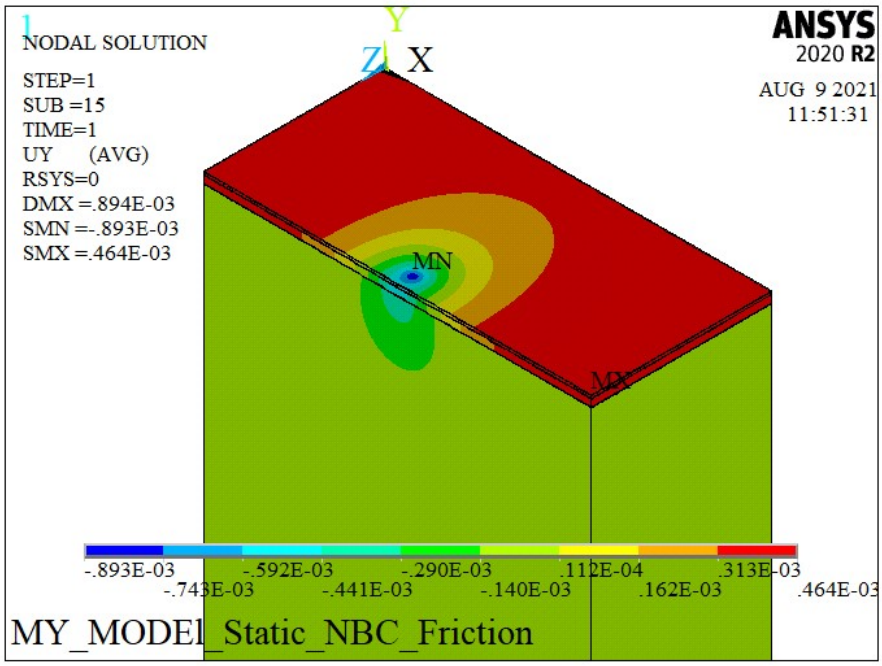

Figure 6.1:.Vertical Displacement (u_y) contour on the frictional pavement model under static loading

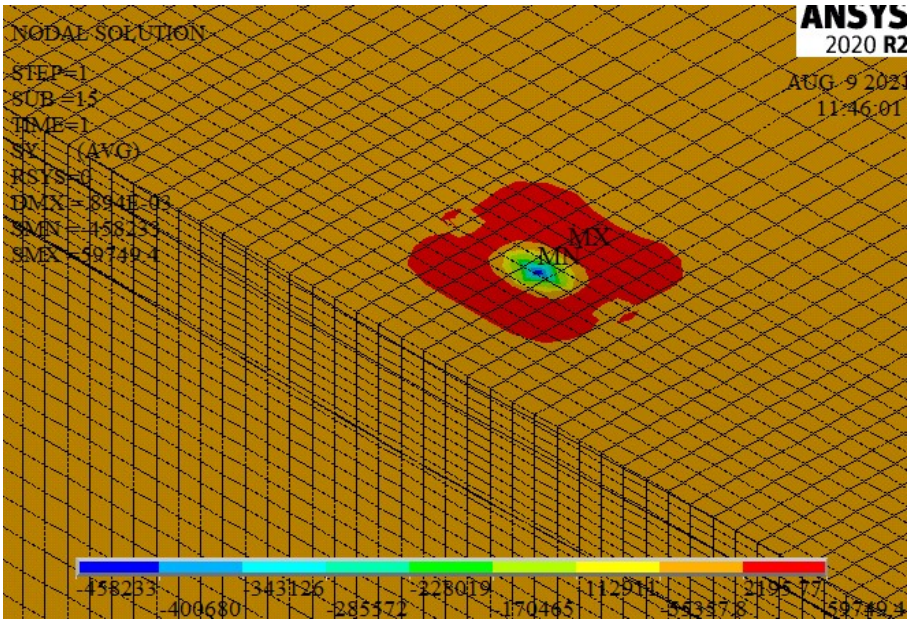

Figure 6.2:.Vertical Stress (σ_y) contour on the frictional pavement model under static loading

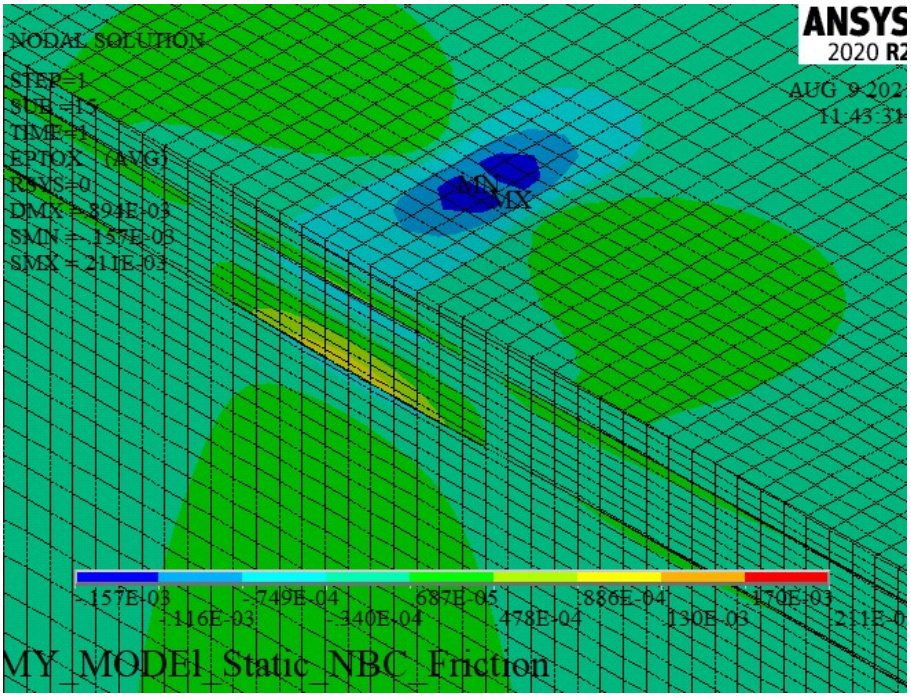

Figure 6.3:.Lateral Strain (ε_z) contour on frictional pavement model under static loading

6.2.2 Dynamic Response Analysis

The model with frictional incorporated in the previous section is further analyzed for dynamic loading. The response of pavement under the different speeds of the standard axle moving on the surface of F.E. pavement is determined, and critical values at the bottom of asphalt (A) and top of subgrade (B) are presented in Table 6.2.

Table 6.2:.Response of Pavement for moving wheel load with friction

v	*y* *(m)*	u_y *(mm)*	σ_y *(kPa)*	ε_y *(x 10^6)*	ε_x *(x 10^6)*	ε_z *(x 10^6)*
5	A(y=0.19m)	-0.5783	-44.68	-	14.18	106.7
	B(y=0.67m)	-0.4162	-12.1	-83.27		
10	A(y=0.19m)	-0.5494	-40.42		13.56	94.21
	B(y=0.67m)	-0.3989	-12.21	-77.35		

Vertical Displacement (u_y) of Pavement

The time history curve for vertical displacement (u_y) at the bottom of asphalt layer (point A) and at the top of subgrade layer (point B) is shown in Figure 6.4. During vehicle travel, the peaks on the curve appear as the wheel axle passes over the location where the response is measured. As in linear finite element analysis, the increase in vehicle speed increases the magnitude of displacement and an earlier appearance of peak displacement in the pavement. The obtained result is understandable given the decrease in vehicle-to-pavement contact time as vehicle speed increases.

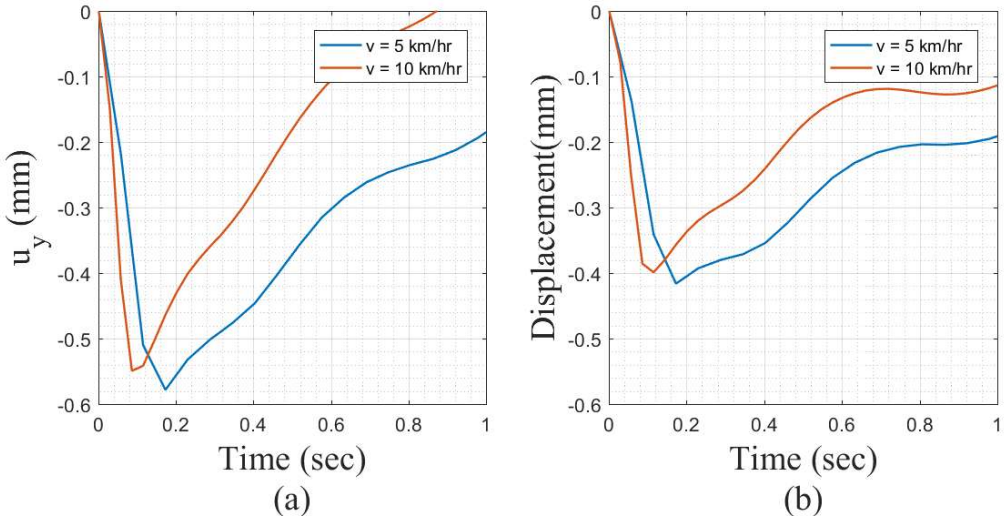

Figure 6.4:.Vertical displacement u_y time history (a) at the bottom of asphalt and (b) at the top of subgrade

Stresses on Pavement

The time history curve for vertical stress(σ_y) at the bottom of the asphalt layer (point A) and at the top of the subgrade layer (point B) is presented in Figure 6.5. The vertical stress (σ_y) decreases by 71 percent on average from point A to point B, compared to 90 percent for the linear model. As the velocity increases in the linear model, the amplitude of vertical stresses in the pavement layers decreases. The reduction in the magnitude of vertical stress at position A is 10% for change speeds of the axle load of 10 km/hr to 5 km/hr, whereas the same at point B is nearly the same. The peak in the time history occurs at the point as the vehicle passes over that point on which response is being recorded. is illustrated in Figure 6.5, the vertical stress (σ_y) on the base-asphalt and subgrade–base interfaces is constantly under compression during the vehicle's travel.

The stress fluctuation is cyclic, and the cycle of change in stress occurs faster as the vehicle's velocity increases. The cyclic pattern of stress decreases at the depth of the pavement.

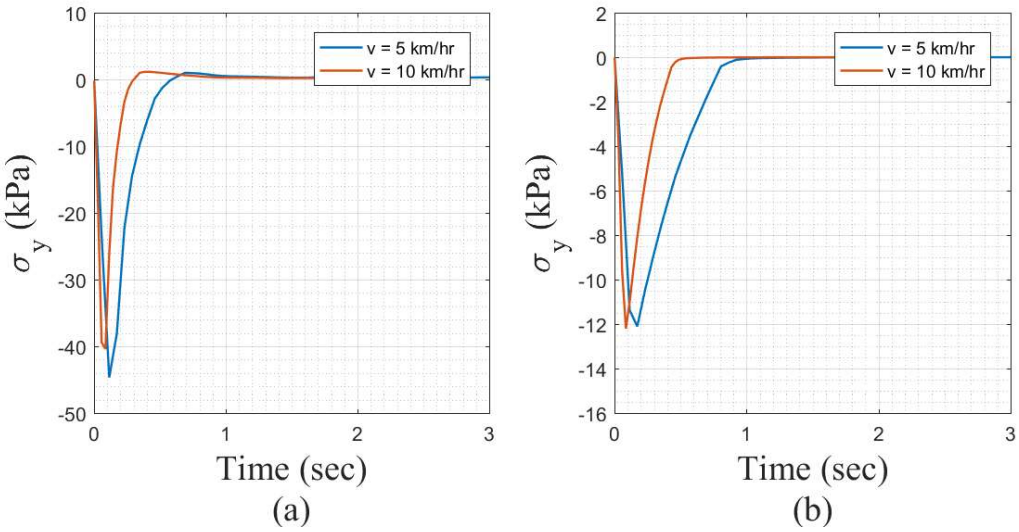

Figure 6.5:.Vertical stress σ_y time history (a) at the bottom of asphalt and (b) at the top of subgrade

Strains on Pavement

The time history curve for vertical strain (ε_y) at the top of the subgrade layer (point A) and lateral strain (ε_z) at the bottom of the asphalt layer (point B) is presented in Figure 6.6. The vertical strain decreases on average by 47 percent from point A to point B for moving axle load at 10 km/hr and 5 km/hr. The magnitude of vertical strains in the pavement layers decreases as the velocity increases, as shown in Table 6.2. The rate of decline is more significant in the upper layers of the pavement, and it has no effect at deeper depths. For speeds of 10 km/hr and 5 km/hr, the reduction in the magnitude of vertical strain at point B is 8%. As illustrated in Figure 5.4, the vertical strain (ε_y) on the base-asphalt(A) and subgrade–base(B) interfaces is always under compression during the vehicle's travel.

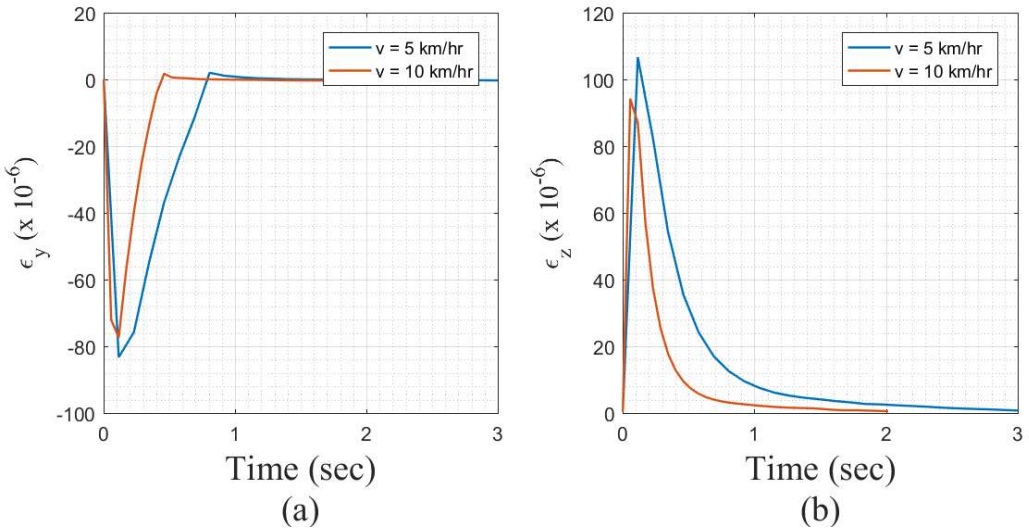

Figure 6.6:.(a) Vertical strain at top of subgrade and (b) horizontal strain at bottom of asphalt

6.2.3 Comparison of response

With the inclusion of friction, the vertical displacement increase; however, the rate of decrease is more significant at the upper layers of the pavement, and the effect is negligible at greater depths. For a 5 km/hr velocity on a standard axle wheel, the response at points A and B increase by 20 percent and 9 percent, respectively, whereas for a velocity of 10 km/hr, the increase is 16 percent and 5 percent. The vertical strain at the top of the subgrade decrease by 170 decrease for friction include the model. The cycle of variation in stress occurs at a quicker rate with an increase in the vehicle's speed, and cyclic variation goes on vanishing with an increase in the depth of the pavement. The lateral strain along the z-axis is in tension along with the depth, is shown in Figure 6.6. The horizontal strain at point A decreases by 35 percent and 80 percent along the x and z directions for axles traveling at 5 km/hr., respectively, and by 36 percent and 77 percent for axles load moving at 10 km/hr.

CHAPTER 7: ACCELERATED LOADING

7.1 General

Analysis and discussion of pavement under vehicle load moving at various speeds have been performed in the previous chapter six to gain insight into road section design and analysis in the near-constant velocity region. In this chapter, accelerated loading analysis is carried out on a finite element pavement model for sections of pavement where accelerated loading is considerable, such as bridge entrants, zebra crossings, converging road sections, start and end of speed limit pavement sections, etc. The effect of accelerated loading has not been studied extensively; thus, one of this thesis's objectives is to propose design guidance for sections where considerably accelerated loading occurs.

Model prepared is trailed with various load step sizes such that the model can capture the accelerated effect. The model can capture response more accurately with a smaller step size; however, it will be more computationally demanding. Thus, a trial is performed to balance accuracy and computational time, and the trial is stopped after obtaining a small difference between the model for increased step size and previous. After which, the model is used for analysis on the various case of accelerated loading. The analysis for accelerated loading is carried out both linear and nonlinear to get a perspective of the magnitude of the difference of response under nonlinear analysis

7.2 Response of pavement considering linear material properties

The pavement FEM model is analyzed with elastic material properties show in Table 4.5 under accelerated loading Table 7.1 contains maximum response obtained from pavement analysis carried out for vehicles moving with the same initial speed deaccelerating with different magnitude to attain the same final speed. The peak on the time history of response is observed on the figure as when load passes over that point. The response determined, shown in the figure, are cyclic; however, with depth, the rate of cyclic nature goes on decreasing. One can observe from Table 7.1 the vertical displacement increase by 1.98% and 1.57% at the bottom of asphalt (point A) and at the top of subgrade layer (point B) for deceleration 2m/s2 compare to 5 m/s2 and the vertical stress reduced by 1.66 percent and 0.37 percent, respectively.

Considering the response of pavement moving with a constant velocity of 10 km/hr, 5km/hr and deaccelerating under 5 m/s2 from 10 km/hr to 5 km/hr, the vertical response at point A decrease by 7.7% and 8.3% for accelerated loading compare to that of

constant velocity loading of 10 km/hr and 5km/hr respectively. While there is an increment in stress and strain for accelerating compare to velocity loading. The vertical stress at the bottom of the asphalt layer is changed by 1.6% and -1% compared to 10 km/hr, and 5 km/hr, respectively, and a similar trend is observed in vertical strain. In the case of horizontal tensile strain (εz) at the bottom of the asphalt layer, there is a magnitude reduction of 0.14% and 0.46% compared to 10 km/hr and 5 km/hr, respectively. On discussing the result, it has been found that strain and stress increase for acceleration when the deacceleration magnitude is faster; however, with slow acceleration magnitude, the response due to slower speed result in higher strain and stress on the pavement.

Table 7.1:.Response of pavement under standard axle load moving with different magnitude of acceleration

Case	*u (km/hr)*	*v (km/hr)*	*a (m/s^2)*	*y(m)*	*u_y (mm)*	*σ_y (kPa)*	*ε_y ($x10^6$)*	*ε_x ($x\ 10^6$)*	*ε_z ($x\ 10^6$)*
1	10	5	-5	A	-0.426	-67.85	-	66.6	-
				B	-0.350	-13.56	-223.9	-	21.62
2	10	5	-2	A	-0.4344	-66.74	-	64.6	-
				B	-0.3559	-13.51	-222.8	-	21.56
3	15	5	-5	A	-0.4436	-67.21	-	62.97	-
				B	-0.3636	-13.53	-221.9	-	21.27
4	15	5	-2	A	-0.4432	-66.72	-	61.84	-
				B	-0.3636	-13.51	-221.3	-	21.22
5	15	10	-5	A	-0.4435	-66.91	-	62.4	-
				B	-0.3638	-13.52	-221.6	-	21.21
6	15	10	-2	A	-0.4433	-66.72	-	61.83	-
				B	-0.3637	-13.51	-221.3	-	21.22
7	20	15	-5	A	-0.4312	-66.21	-	60.12	-
				B	-0.3543	-13.48	-220.2	-	20.96
8	20	15	-2	A	-0.4426	-65.82	-	59.11	-
				B	-0.3638	-13.45	-219.5	-	20.91

Note: u – initial velocity; v- final velocity; a - acceleration

7.3 Response of pavement considering friction

From the result and discussion of the previous chapter, it has been found out that there is a significant difference in the frictional model's response compared to the response of pavement analysis with the bonded model for constant velocity loading. To find out what may be the case for accelerated loading, the analysis of pavement is carried out.

The linear elastic properties of Table 4.5 are used in the finite element model. The friction interface is considered between asphalt-base and base-subgrade interface with a coefficient of friction of 0.15. The accelerated standard wheel axle is moved on the surface of the pavement, and the result has been determined. Table 7.2 contains the maximum response of pavement under accelerating load with friction inclusion. As in constant velocity loading, the peak on the time history of response occurs when load passes over that point. The response determined, shown in Figure 7.1-Figure 7.3, are cyclic in nature; however, with depth, the rate of cyclic nature goes on decreasing.

Table 7.2:.Response of frictional pavement model under accelerated loading

u (km/hr)	v (km/hr)	a (m/s^2)	y(m)	u_y (mm)	σ_y (kPa)	ε_y ($x10^6$)	ε_x ($x\ 10^6$)	ε_z ($x\ 10^6$)
10	5	-5	A	-0.7339	-227		182.2	223.7
			B	-0.4946	-18.97	-142.5	182.2	
		-2	A	-0.726	-221.3		176.8	220.4
			B	-0.4898	-18.98	-141.7		

Table 7.2 shows that with a decrease rate of deceleration (2 m/s^2 from 5 m/s^2), the vertical displacement decreases by 1% and 0.98% at points A and B, respectively. The magnitude of vertical stress decrease by 2.58% at point A and a similar trend is observed for vertical strain; the strain decreased by 0.56% at point B. The horizontal tensile strain at point A decreases by 3% and 1.5% along x and z directions, respectively.

The comparison of the pavement response for accelerating load to that of constant velocity loading is performed to get insight into the effect of acceleration. As a representative example, the response of deceleration wheel load under 5 m/s^2 from 10 km/hr to 5 km/hr and response under constant moving wheel load 10 km/hr and 5 km/hr are taken. The vertical displacement under deaccelerating loading increase by 25% and 21% compared to the response of constant axle loading moving with 10 km/hr and 5 km/hr respectively at point A while 19% and 15% at point B. As opposed to the response in linear accelerating loading, under acceleration, stress and strain increase compare to constant velocity. The vertical stress is increased by 82% at point A and 35% at point B. There is an increment of 42% on average for vertical strain at point B under accelerated loading and 92% increment in the strain at point A for horizontal tensile strain.

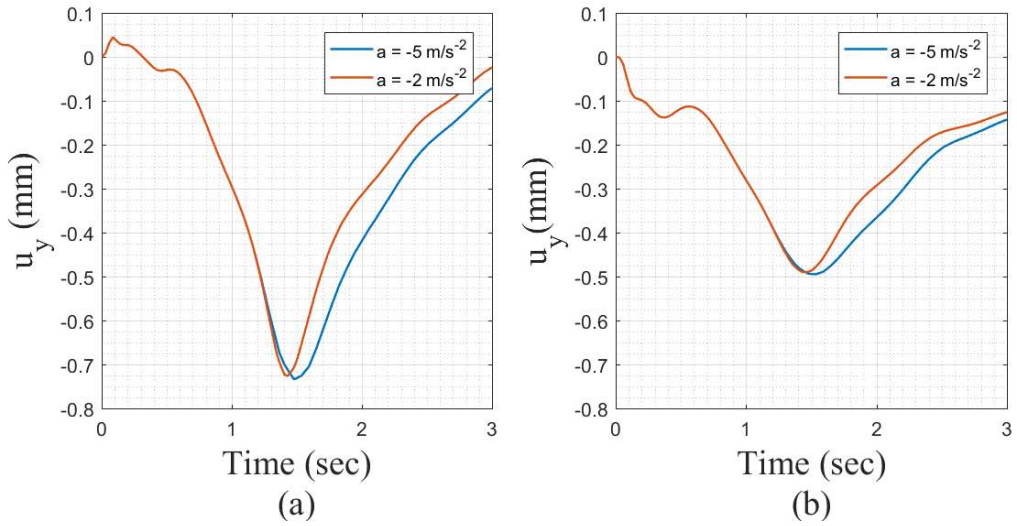

Figure 7.1:.Vertical displacement (u_y) under deacceleratd vehicular loading (a) at the bottom of asphalt and (b) at the top of subgrade

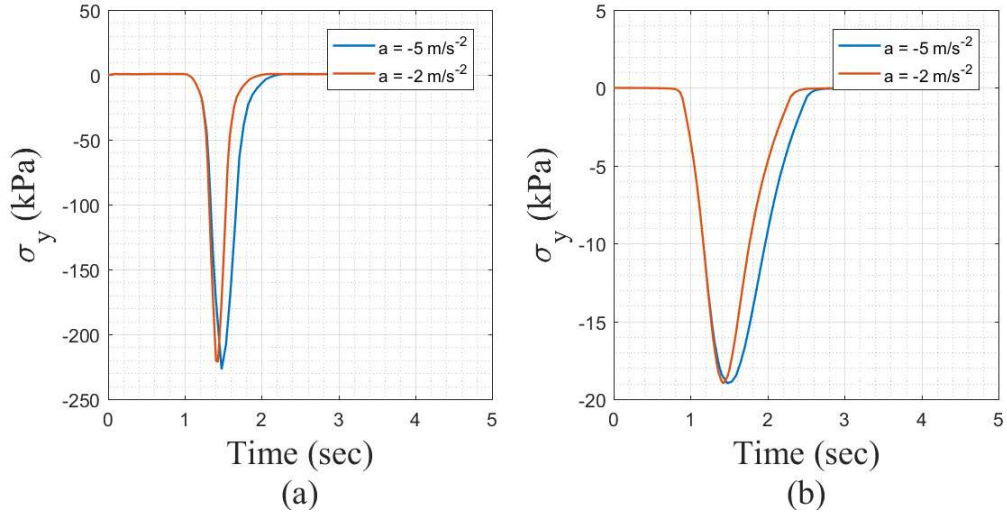

Figure 7.2:.Vertical stress (σ_y) under deaccelerated vehicular loading (a) at the bottom of asphalt and (b) at the top of subgrade

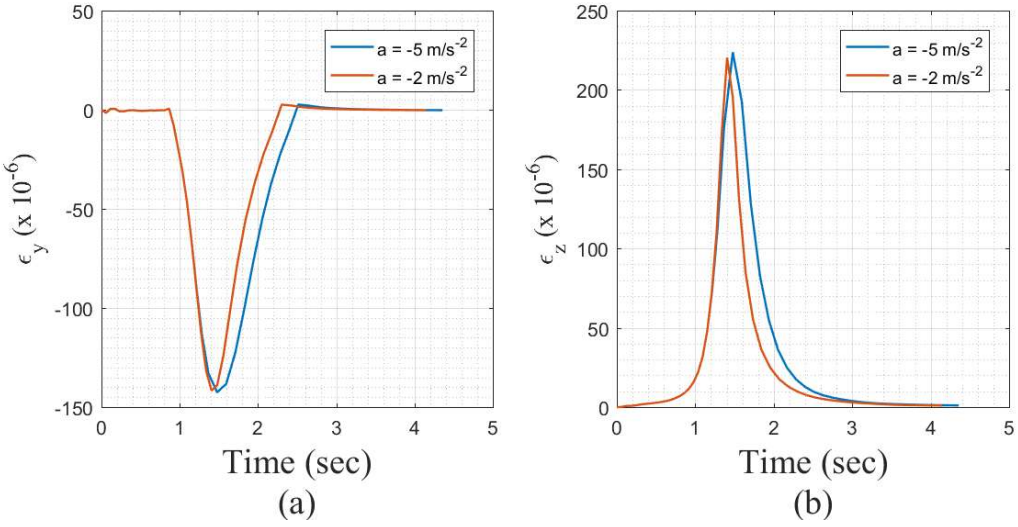

Figure 7.3:.(a) Vertical strain (ε_y) under deaccelerated vehicular loading at the top of subgrade and (b) Lateral strain (ε_z) at the bottom of asphalt

7.4 Response of pavement considering nonlinear material properties

Asphalt in nature shows rate-dependent loading response, and inclusion of this property in the FEM model results in more reality to nature. Beskou, Hatzigeorgiou, et al. (2016) have shown that pavement response with linear material has a difference in the response compared to the nonlinear material response. Beskou, Hatzigeorgiou, et al. (2016); Assogba et al., (2020). etc., have used the viscoelastic constitutive model in F.E. simulation. This thesis is carried out, including the viscoelastic model for pavement for accelerated loading.

Table 4.6**Error! Reference source not found.** contains viscoelastic material properties taken for pavement simulation. The response of pavement with a viscoelastic constitutive model is presented in Table 7.4 for decelerated standard axle load. With the inclusion of nonlinear material properties in pavement simulation, the response of pavement increase/decrease but have in nature to that in linear modeling.

Table 7.3:.Nonlinear Response of pavement under constant vehicular speed

u (km/hr)	*y(m)*	u_y *(mm)*	σ_y *(kPa)*	ε_y *(x10⁶)*	ε_x *(x 10⁶)*	ε_z *(x 10⁶)*
5	A (y=0.19m)	-0.7339	-227		182.2	223.7
	B (y=0.67m)	-0.4946	-18.97	-142.5		
10	A (y=0.19m)	-0.726	-221.3		176.8	220.4
	B (y=0.67m)	-0.4898	-18.98	-141.7		

Table 7.4:.Nonlinear Response of pavement under accelerated laoding

u (km/hr)	v (km/hr)	a (m/s^2)	y(m)	u_y (mm)	σ_y (kPa)	ε_y ($x10^6$)	ε_x ($x\ 10^6$)	ε_z ($x\ 10^6$)
10	5	-5	A	-0.4856	-221.8		108.2	146
			B	-0.3687	-15.38	-257.2		
		-2	A	-0.5004	-220.8		107.5	145.5
			B	-0.378	-15.37	-257.1		

Note: u – initial velocity; v- final velocity; a - acceleration

Vertical Displacement (u_y) of Pavement

The time history of vertical displacement at the critical point, i.e., the bottom of the asphalt layer (point A) and top of subgrade point (B) is shown in Figure 7.4. The displacement of pavement is in the direction of pressure, and with the increase in depth, the displacement decreases. One can observe from Table 7.4, the increase in magnitude of deacceleration from 2 m/s2 to 5 m/s2 the peak vertical displacement increase by 3% and 2.5% at the point A and point B, respectively. The cyclic nature of response goes on decreasing along the depth of the pavement. The rate of increase is more significant at the upper layers of the pavement and the effect is decreasing along the depths of pavement.

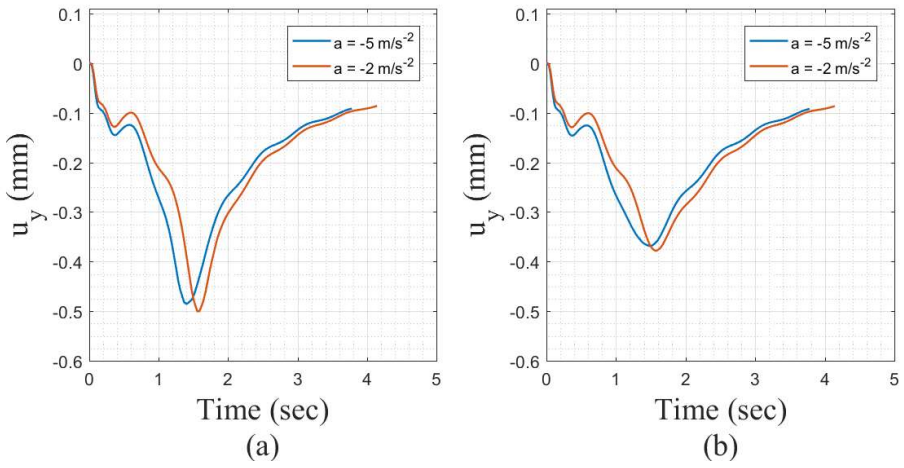

Figure 7.4:.Vertical displacement (u_y) under deacceleratd vehicular loading (a) at the bottom of asphalt and (b) at the top of subgrade

Stresses on Pavement

The time history curve of vertical stress (σ_x) at the critical point, i.e., the bottom of the asphalt layer (point A) and top of subgrade point (B) is shown in Figure 7.5. The difference in vertical stress is under 1% for deaccelerating vehicular with the magnitude of 2 m/s2 and 5 m/s2 measured at point A and point B. The vertical stress is compressive in nature at rate of increasing goes on decrease along the depth of pavement.

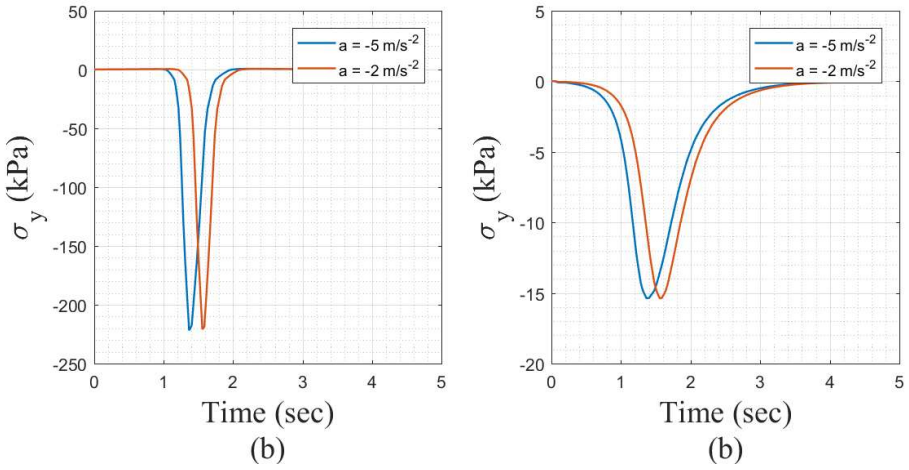

Figure 7.5:.Vertical stress (σ_y) under deacceleratd vehicular loading (a) at the bottom of asphalt and (b) at the top of subgrade

Strains on Pavement

The time history curve of vertical strain (ε_y) at top of subgrade and lateral strain (ε_z) at bottom of asphalt layers is shown in Figure 7.6. The peak observed on the time history curve on point when vehicle load passed over that point. With increase in magnitude of deaccelearating the peak of response occurs eairlies The nature of vertical strain at point A and point B is compressive while lateral strain is tensile.

The reduction in magnitude of vertical stress at point A is 31% for speeds of 20 m/s and 5 m/s and the same at point B was 15% increment. Here also, it can be observed that the two peaks also occur on the stresses time history due to tandem wheel configuration. The vertical strain (ε_y) on base-asphalt and subgrade–base interface is always on compression during entire motion of the vehicle as shown in Figure 5.3.

There is in average of 93 % decrease in strain ε_z respectively from point A to point B. Further, Table 7.4 shows that with the increase in the velocity the magnitude of tensile

strains in the pavement layers goes on decreasing. The rate of decrease is more significant at the upper layers of the pavement and the effect is negligible at higher depths. The reduction in magnitude of stress (ε_z) at point A is 7%, for speeds of 20 m/s and 5 m/s respectively as shown in Figure 7.6.

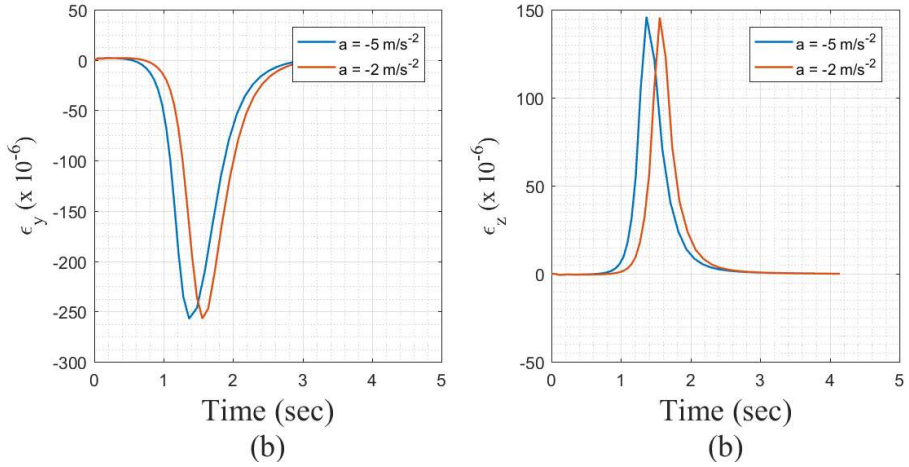

Figure 7.6:.(a) Vertical strain (ε_y) under deaccelerated vehicular loading at the top of subgrade and (b) Lateral strain (ε_z) at the bottom of asphalt

7.5 Comparison of Responses

From the results in Table 7.1 and Table 7.4 it is observed that the nonlinear response of pavement results in higher response (displacement,stress and strain) in comparison to linear response under accelerated loading. For nonlinear response, the vertical displacement at bottom of asphalt is about 19 % larger and at top of subgrade, it is about 12 % larger than linear response. However, the vertical stress at bottom of asphalt and lateral strain at top of subgrade is significantly higher for nonlinear response i.e 70% and 85 % respectively.

For non-linear analysis, the vertical displacement under deaccelerated loading (5m/s^2) is about 8% less than response of pavement for constant velocity . The maximum stress on pavement under accelerated loading is lesser than the constant velocity loading (5km/hr). The magnitude of change is found to be decreasing with depth. At point A (y=0.19m) the change is 1.8% whereas at point B (y=0.67m), the change is 0.7%. The strain also follow similar trend as stress. The lateral strain at point A is 1.5% lower for deaccelerated loading.

However, the lateral stress at point A is 2.9% higher and at point B, it is 0.39% higher for deaccelerated loading than the stress with uniform velocity (10km/hr). The strain also follows same trend as stress. The lateral strain at point A is 3% higher for deaccelerated loading. The result could be used for designing purpose based on iterative modeling of section for economical and safe design by performing parametric study.

CHAPTER 8: CONCLUSION AND RECOMMENDATION

The three-dimensional finite element model of pavement is simulated in the ANSYS Mechanical APDL, with the validated finite element model subjected to various loading parameters to understand the pavement's response. The developed model is capable of simulating the response of a flexible pavement subjected to vehicular loading. The analysis is carried out, and a thorough discussion is made to understand the effect of vehicular motion with different velocities/accelerations on stresses and strains experienced by the pavement, particularly for Nepalese conditions, which have not been documented yet.

8.1 Conclusions

Based on results and discussion for velocity and acceleration loading in the flexible pavement, the following conclusions are made:

1. The tata motor, LPK 6S, vehicle is modeled with three spatial distribution of wheel i) series of distributed pressure ii) series of concentrated forces, and iii) a concentrated point force each having same resultant force of 250 KN. The response of the pavement under the concentrated load is found to be higher than under series of distributed pressure loads and concentrated load; however, the variation between them is not much (under 20%). For the simplicity of modeling, a concentrated load can be used in the analysis without much effect on the result of the analysis.
2. The dynamic response of pavement for constant speed vehicular loading decreases with the increase in the speed of a vehicle as the contact time of the vehicle on pavement surface decreases. This is understandably due to the reduction of vehicle and pavement contact time with the vehicle's increment in speed for both linear and nonlinear material. The stress-strain variation is cyclic, and the cycle of variation in stress occurs faster with an increase in the vehicle's speed.
3. The inclusion of friction in FEM pavement represents more to the realistic nature of pavement with which the computation becomes more demanding due to frictional nonlinearity. The vertical displacement has increased while the stress and strain have decreased compared to the bonded model for linear material. For a 5 km/hr velocity on a standard axle wheel, the response at bottom of asphalt and top of subgrade increase by 20 percent and 9 percent,

respectively, whereas for a velocity of 10 km/hr, the increase is 16 percent and 5 percent between frictional and bonded pavement model.

4. Elastic models, particularly static ones, considerably underestimate the real pavement response and should thus be utilized with caution in design.
5. A comparison of elastic and viscoelastic models under vehicle loads moving at constant speed indicated that viscoelastic models have a greater reaction than elastic ones. The vertical stress-strain at the top of the subgrade increased by 11% and 13%, respectively, whereas the lateral stress at the bottom of the asphalt increased by 86% (for a speed range of 5km/hr -10km/hr).
6. It was found that nonlinear model produce response result always higher than the corresponding elastic loading under accelerated vehicular loading. The vertical displacement at bottom of asphalt is about 19 % and 12 % larger for nonlinear response. The vertical stress at bottom of asphalt and lateral strain at top of subgrade is significantly different for nonlinear response , about 70% and 85% respectively.
7. A comparison between maximum response during constant velocity and deaccelerated loading, the maximum stress on pavement under deaccelerated loading (with 5 m/s^2 from 10km/hr to 5 km/hr) is lesser than the constant velocity loading (5km/hr). The magnitude of change is found to be decreasing with depth. At bottom of asphalt (y=0.19m) the change is 1.8% whereas at top of subgrade (y=0.67m), the change is 0.7%. The lateral strain at asphalt's bottom is 1.5% lower for deaccelerated loading. However, the lateral stress at point asphalt's bottom is 2.9% higher and at subgrade's top, it is 0.39% higher for deaccelerated loading than the stress with uniform velocity (10km/hr). The lateral strain at asphalt's bottom is 3% higher for deaccelerated loading.

8.2 Recommendation

The recommendation for the future work

1. The research work have been done for limited vehicular speed and acceleration which can extend for large range and can produced empirical relationship.
2. Having determined the maximum stress and strain, the work can be used in the further analysis for rutting and fatigue of the pavement.
3. The pavement can be model with a futher better constitutive material model for a more accurate representation of pavement response

REFERENCES

AASHTO Guide for Design of Pavement Structures (1993, American Association of State Highway and Transportation Officials (AASHTO)). (n.d.).

Al-Qadi, I. L., Wang, H., Yoo, P. J., & Dessouky, S. H. (2008). Dynamic Analysis and in Situ Validation of Perpetual Pavement Response to Vehicular Loading. *Transportation Research Record: Journal of the Transportation Research Board*, *2087*(1), 29–39. https://doi.org/10.3141/2087-04

Ali, B., Sadek, M., & Shahrour, I. (2009). Finite-Element model for urban pavement rutting: Analysis of pavement rehabilitation methods. *Journal of Transportation Engineering*, *135*(4), 235–239. https://doi.org/10.1061/(ASCE)0733-947X(2009)135:4(235)

Arros, J. K. (2002). Dynamics of structures. In *Earthquake Engineering Handbook* (pp. 3-1-3–40). https://doi.org/10.1139/l90-078

Assogba, O. C., Tan, Y., Zhou, X., Zhang, C., & Anato, J. N. (2020). Numerical investigation of the mechanical response of semi-rigid base asphalt pavement under traffic load and nonlinear temperature gradient effect. *Construction and Building Materials*, *235*, 117406. https://doi.org/10.1016/j.conbuildmat.2019.117406

Bathe K J. (2005). Finite Element Procedures [M]. In *Englewood Cliffs New Jersey*.

Berthelot, C. F., Allen, D. H., & Searcy, C. R. (2003). Method for Performing Accelerated Characterization of Viscoelastic Constitutive Behavior of Asphaltic Concrete. *Journal of Materials in Civil Engineering*, *15*(5), 496–505. https://doi.org/10.1061/(asce)0899-1561(2003)15:5(496)

Beskou, N. D., Hatzigeorgiou, G. D., & Theodorakopoulos, D. D. (2016). Dynamic inelastic analysis of 3-D flexible pavements under moving vehicles: A unified FEM treatment. *Soil Dynamics and Earthquake Engineering*, *90*, 420–431. https://doi.org/10.1016/j.soildyn.2016.09.018

Beskou, N. D., & Theodorakopoulos, D. D. (2011). Dynamic effects of moving loads on road pavements: A review. *Soil Dynamics and Earthquake Engineering*, *31*(4), 547–567. https://doi.org/10.1016/j.soildyn.2010.11.002

Beskou, N. D., Tsinopoulos, S. V., & Theodorakopoulos, D. D. (2016). Dynamic elastic analysis of 3-D flexible pavements under moving vehicles: A unified FEM treatment. *Soil Dynamics and Earthquake Engineering*, *82*, 63–72. https://doi.org/10.1016/j.soildyn.2015.11.013

Boussinesq, J. (1885). *Application des potentiels*. http://quod.lib.umich.edu/u/umhistmath/abv5032.0001.001/1?view=pdf

Burmister, D. M. (1945). The general theory of stresses and displacements in layered soil systems. II. *Journal of Applied Physics*. https://doi.org/10.1063/1.1707562

Cebon, D. (1999). *Handbook of vehicle-road interaction.*

Cho, Y.-H., McCullough, B. F., & Weissmann, J. (1996). Considerations on Finite-Element Method Application in Pavement Structural Analysis. *Transportation Research Record: Journal of the Transportation Research Board*, *1539*(1), 96–101. https://doi.org/10.1177/0361198196153900113

DeSalva, Gabriel J., Swanson, J. A. (1985a). *ANSYS engineering analysis system user's manual*. Houston, Pa. :Swanson Analysis Systems.

DeSalva, Gabriel J., Swanson, J. A. (1985b). *ANSYS Mechanical APDL Basic Design Guide*. Houston, Pa. :Swanson Analysis Systems.

DOR. (2014). *Pavement Design Guidelines (Flexible Pavement)*.

González, J. M., Miquel Canet, J., Oller, S., & Miró, R. (2007). A viscoplastic constitutive model with strain rate variables for asphalt mixtures-numerical simulation. *Computational Materials Science*, *38*(4), 543–560. https://doi.org/10.1016/j.commatsci.2006.03.013

Gungor, O. E., Al-Qadi, I. L., Gamez, A., & Hernandez, J. A. (2016). In-situ validation of three-dimensional pavement finite element models. In *The Roles of Accelerated Pavement Testing in Pavement Sustainability: Engineering, Environment, and Economics* (pp. 145–159). Springer International Publishing. https://doi.org/10.1007/978-3-319-42797-3_10

Howard, I. L., & Warren, K. A. (2009). Finite-element modeling of instrumented flexible pavements under stationary transient loading. *Journal of Transportation Engineering*, *135*(2), 53–61. https://doi.org/10.1061/(ASCE)0733-947X(2009)135:2(53)

Huang, B., Mohammad, L. N., & Rasoulian, M. (2001). Three-dimensional numerical simulation of asphalt pavement at Louisiana accelerated loading facility. *Transportation Research Record*, *1764*(1764), 44–58. https://doi.org/10.3141/1764-06

Huang, C.-W., Abu Al-Rub, R. K., Masad, E. A., & Little, D. N. (2011). Three-Dimensional Simulations of Asphalt Pavement Permanent Deformation Using a Nonlinear Viscoelastic and Viscoplastic Model. *Journal of Materials in Civil*

Engineering, *23*(1), 56–68. https://doi.org/10.1061/(asce)mt.1943-5533.0000022

Huang, Y. H. (2004). Pavement Analysis and Design, Prentic–Hall. In *Inc., New Jersey: Vol. Highway Re*.

Koti Marg, K., & Puram, R. (2018). *GUIDELINES FOR THE DESIGN OF FLEXIBLE PAVEMENTS INDIAN ROADS CONGRESS*.

Li, M., Wang, H., Xu, G., & Xie, P. (2017). Finite element modeling and parametric analysis of viscoelastic and nonlinear pavement responses under dynamic FWD loading. *Construction and Building Materials*, *141*, 23–35. https://doi.org/10.1016/j.conbuildmat.2017.02.096

Li, S., Guo, Z., & Yang, Y. (2016). Dynamic viscoelastic response of an instrumented asphalt pavement under various axles with non-uniform stress distribution. *Road Materials and Pavement Design*, *17*(2), 446–465. https://doi.org/10.1080/14680629.2015.1080178

Lu, Y., & Wright, P. J. (1998). Numerical approach of visco-elastoplastic analysis for asphalt mixtures. *Computers and Structures*, *69*(2), 139–147. https://doi.org/10.1016/S0045-7949(98)00139-4

Note-31, R. (1984). *Road note 31: a guide to the structural design of bitumen surfaced roads in tropical and subtropical countries*.

Odemark, S. N. (1949). Investigations as to the Elastic Properties of Soils and Design of Pavements According to the Theory of Elasticity. In *Statens Vaginstitut /Sweden/*.

PAVEMENT, V. M. O. F., To, A. D. P., Fulfillment, T. G. F. of T. U. of A. I. P., Philosophy, of the R. for the D. D. of, & Chen, Y. (2009). VISCOELASTIC MODELING OF FLEXIBLE PAVEMENT. *Aspectos Generales De La Planificación Tributaria En Venezuela*, *2009*(75), 31–47.

Saint-Venant, B. D. (1855). *Mémoire sur la torsion des prismes. Mémoires des Savants étrangers*. *233–560*.

Saleeb, A., Liang, R. Y., Qablan, H. A. L., & Powers, D. (2005). Numerical simulation techniques for HMA rutting under loaded wheel tester. *International Journal of Pavement Engineering*, *6*(1), 57–66. https://doi.org/10.1080/10298430500068704

Shen, W., & Kirkner, D. J. (2001). Non-linear Finite-Element Analysis to Predict Permanent Deformations in Pavement Structures Under Moving Loads. *International Journal of Pavement Engineering*, *2*(3), 187–199. https://doi.org/10.1080/10298430108901726

Tata-Motar *LPK 2518 6S*, July 2020 < URL: https://tatatrucks.tatamotors.com/tata-trucks/tippers/tata-lpk-2518/tata-lpk-2518-6s-20cum-specifications.aspx#specifications>

Yoo, P. J., & Al-Qadi, I. L. (2007). Effect of transient dynamic loading on flexible pavements. *Transportation Research Record*, *1990*(1990), 129–140. https://doi.org/10.3141/1990-15

Zaghloul, S., White, T., Drnevich, V., & Coree, B. (1994). Dynamic analysis of FWD loading and pavement response using a three-dimensional dynamic finite-element program. *ASTM Special Technical Publication, 1198*, 125–125.

ANNEX A: ANSYS APDL Code for Finite Element Model

```
! *** BEGIN OF MODEL***
! *** Build the Model *****
/CWD,'E:\Bijay Ban\CIDS\Ansys\TRY'    ! DIRECTORY FOR GEOMETRY

! GEOMETRY PARAMETER
/INPUT,'Nepal Model_2','txt','E:\Bijay Ban\CIDS\Ansys_C'
        XSIZE = 0.23/2
/TITLE,MY LAYERED ELASTIC MODEL

! *** PREPROCESSOR MODULUS
/PREP7
        ! MATERIAL PROPERTIES
        /INPUT,'Nepal Road Properties','txt','E:\Bijay Ban\CIDS\Ansys_C'

        ! **** Keypoint for the mode ****
        ! Asphalt layer keypoint
        *Do,I,1,4,1
        *IF,I,EQ,1,then
        DIS = 0
        A =0
        *ELSEIF,I,EQ,2,then
        DIS = -CD
        A= 20
        *ELSEIF,I,EQ,3,then
        DIS = -CD-DF
        A = 40
        *ELSE
        DIS = -CD-DF-FG
        A = 60
        *ENDIF


        K,A+1,0,DIS,0
        K,A+2,OA,DIS,0
        K,A+3,OA+AQ,DIS,0
        K,A+4,OA+2*AQ,DIS,0
        K,A+5,2*OA+2*AQ,DIS,0

        K,A+6,0,DIS,OC
        K,A+7,OA,DIS,OC
        K,A+8,OA+AQ,DIS,OC
        K,A+9,OA+2*AQ,DIS,OC
        K,A+10,2*OA+2*AQ,DIS,OC

        K,A+11,0,DIS,OC+Z2
        K,A+12,OA,DIS,OC+Z2
        K,A+13,OA+AQ,DIS,OC+Z2
        K,A+14,OA+2*AQ,DIS,OC+Z2
        K,A+15,2*OA+2*AQ,DIS,OC+Z2
```

```
K,A+16,0,DIS,OC+Z1+Z2
K,A+17,OA,DIS,OC+Z1+Z2
K,A+18,OA+AQ,DIS,OC+Z1+Z2
K,A+19,OA+2*AQ,DIS,OC+Z1+Z2
K,A+20,2*OA+2*AQ,DIS,OC+Z1+Z2
*ENDDO                                  ! END DO I

! **** Generate Line for the modal ****
B = 0
*Do, k,1,4,1                            ! For lines across depth
*Do,I,1,5,1                             ! For lines acrooss length 4 + 1

*IF,I,eq,1,then
A = 0
*Do,j,1,4,1
*if,j,LT,3,THEN                         ! For normality of lines
L,j+A+B,j+A+B+1
*Else
L,j+A+B+1,j+A+B
*ENDIF
*ENDDO                                  ! END DO J

*ELSEIF,I,eq,2
A = 5
*Do,j,1,4,1
*if,j,LT,3,then
L,j+A+B,j+A+B+1
*Else
L,j+A+B+1,j+A+B
*ENDIF
*ENDDO                                                  ! END DO J

*ELSEIF,I,eq,3
A = 10
*Do,j,1,4,1
*if,j,LT,3,then
L,j+A+B,j+A+B+1
*Else
L,j+A+B+1,j+A+B
*ENDIF
*ENDDO                                                  ! END DO J

*ELSEIF,I,eq,4
A = 15
*Do,j,1,4,1
*if,j,LT,3,then
L,j+A+B,j+A+B+1
*Else
L,j+A+B+1,j+A+B
```

```
*ENDIF
*ENDDO                                          ! END DO J

*Else
A1 = 5
A2 = 10
A3 = 15
*Do,j,1,5,1
L,j+B,j+A1+B
L,j+B+5,j+A2+B
L,j+B+10,j+A3+B
*ENDDO                                  ! END DO J
*ENDIF
*ENDDO                                  ! END DO I LENGTH
B = B + 20
*ENDDO                                  ! END DO K DEPTH

*DO,I,1,3,1                             ! vertical line across depth
*IF,I,EQ,1,THEN
A = 0
*ElSEIF,I,EQ,2,THEN
A = 20
*ELSE
A = 40
*ENDIF
*DO,J,1,5,1
L,A+J,A+J+20
L,A+5+J,A+25+J
L,A+10+J,A+30+J
L,A+15+J,A+35+J
*ENDDO                                   ! END DO J
*ENDDO                                   ! END DO I

! *** Generation of Volume Element ***
*Do,j,1,3,1
*IF,J,EQ,1,THEN
A = 0
*ELSEIF,J,EQ,2,THEN
A = 20
*ELSE
A = 40
*ENDIF
*Do,I,1,4,1
V,I+A,I+A+1,I+A+6,I+A+5,I+A+20,I+A+21,I+A+26,I+A+25
V,I+A+5,I+A+6,I+A+11,I+A+10,I+A+25,I+A+26,I+A+31,I+A+30
V,I+A+10,I+A+11,I+A+16,I+A+15,I+A+30,I+A+31,I+A+36,I+A+35
*ENDDO                                  ! END DO J
*ENDDO                                  ! END DO I

! *** Meshing of pavement ***
```

```
Lsel,s,length,,z1
Lesize,all,,,nod_z1
Lsel,s,length,,z2
Lesize,all,,,nod_z2

Lsel,s,length,,OA
Lesize,all,,,nod_OA,space_OA
Lsel,s,length,,AQ
Lesize,all,,,AQ/XSIZE,1


Lsel,s,length,,OC
Lesize,all,,,nod_OC,space_OC
Lsel,s,length,,CD
Lesize,all,,,nod_CD
Lsel,s,length,,DF
Lesize,all,,,nod_DF
Lsel,s,length,,FG
Lesize,all,,,nod_FG,space_FG

Allsel,all
Type,1
Mat,1                                   !Layered half space
Vmesh,1,12,1
MAT,2
VMESH,13,24,1
MAT,3
VMESH,25,36,1

! *** LOADPATH NODE ***

NSEL,S,LOC,X,OA,OA+AQ+AQ
NSEL,R,LOC,Z,OC+2*ZSIZE
NSEL,R,LOC,Y,0
CM,FLOADPATH,NODE
*GET,num,NODE,,COUNT
Allsel,All
N,FLNODS,OA,0,OC+2*ZSIZE
                                        ! FLNODS 1000000
N,FLNODS+NUM-1,OA+AQ+AQ,0,OC+2*ZSIZE
                                        ! END OF FLNODS
N,SLNODS,OA,0,OC+3*Zsize                ! SLNODS 1000200
N,SLNODS+NUM-1,OA+AQ+AQ,0,OC+3*ZSIZE
                                        ! END OF SLNODS
N,TLNODS,OA,0,OC+4*ZSIZE                ! TLNODS 1000000
N,TLNODS+NUM-1,OA+AQ+AQ,0,OC+4*ZSIZE
                                        ! END OF TLNODS
N,FONODS,OA,0,OC+5*Zsize                ! FONODS 1000200
N,FONODS+NUM-1,OA+AQ+AQ,0,OC+5*ZSIZE
```

```
                                                    ! END OF FONODS

        ! ***FILLING OF NODS BETEWEEN START AND END OF NODS

        FILL,FLNODS,FLNODS+num-1,num-2,FLNODS+1,1,1,1,1,
        FILL,SLNODS,SLNODS+num-1,num-2,SLNODS+1,1,1,1,1,
        FILL,TLNODS,TLNODS+num-1,num-2,TLNODS+1,1,1,1,1,
        FILL,FONODS,FONODS+num-1,num-2,FONODS+1,1,1,1,1,
        NUMMRG,NODE,0.01,,,HIGH

        ! *** To Constraint Nodes Between Layers ***
        ALLSEL,ALL
        Nsel,S,Loc,X,OQ
        Nsel,A,Loc,X,OQ + QB
        CM,mnodes,Node
        Nummrg,Node,TOL,,,

        ! ** Boundary Conditons Xroll , Yroll and Zroll

        ASEL,s,loc,x,0
        ASEL,a,loc,x,2*OA+2*AQ
        NSLA,s,1
        CM,xroll,node
        ASEL,s,loc,z,0
        ASEL,a,loc,z,OC+Z2+Z1
        NSLA,s,1
        CM,zroll,node
        ASEL,s,loc,y,-CD-DF-FG
        NSLA,s,1
        CM,yroll,node
        Allsel,all
        EPLOT
        /VIEW,1,1,1,1
        /REP
FINISH
```

ANNEX B: Transient Analysis for Accelerated Loading

```
/BATCH
! *** BEGIN OF MODEL***
!***CASE I DeAccelerated Loading-SERIES OF DISTRIBUTED LOADING
! *** /INPUT,'MY_TRMODEL_C1_ACC','txt','F:\CIDS\Ansys'

! *** GEOMETRY MODULUS
/INPUT,'MY_MODEL_AMF','txt','F:\CIDS\Ansys'

! *** SOLUTION MODULUS
/CWD,'C:\Result'          ! SOLU DIRECTORY

! *** Data to modify for different run
!*****************************************
/FILNAME,TR_1_10_5_ACC        ! deaccelerating from 20 to 10
Snode =  15                                   ! STR OF VEHICLE STW 0
FW AT S+43
I_Vel_kmhr = 10.00                                ! INITIAL VELOCITY
F_Vel_kmhr = 05.00                                ! FINAL VELOCITY
INITIAL_DIST = 20*XSIZE                ! FOR INITAL DISTANCE TO
ACHIVE VELOCITY
ACC_DIST     = 09*xsize     ! DISTANCE TO ACHIVE FINAL VELOCITY
FINAL_DIST  = 20*xsize     ! DISTANCE TO ACHIVE FINAL VELOCITY
ACC                  = -5                         ! ACCELERATION VALUE
RUN_No = 49
! *****************************************

/TITLE,MY TRANSISENT DEACCELERATING MODEL

/SOL                              ! enter solution
ANTYPE,trans                      ! transient analysis
OUTRES,NSOL,LAST
trnopt,full                              ! full method
ALPHAD,0.159224                          ! Mass damping
BETAD,0.014223                                ! Stiffness damping

ALLSEL,ALL
! Applying Roller Boundaries
EPLOT
CMSEL,S,zroll
D,all, , , , , ,uz
CMSEL,S,xroll
D,all, , , , , ,ux
CMSEL,S,yroll
D,all, , , , , ,uy                ! constraints
allsel,all



! Applying Load At Node One At A Times
```

```
PRES1 = 4E4/(4*XSIZE*ZSIZE)                    !          TANDAM
WHEEL190/8 KN
I_Vel = I_Vel_kmhr*(5/18)
F_Vel = F_Vel_kmhr*(5/18)
FINIAL_DIST  = INITIAL_DIST + ACC_DIST
TIME_1 = XSIZE/I_Vel
TIME_2 = XSIZE/F_Vel

! NBC wheel half only
        ALLSEL,ALL
        NSEL,S,NODE,,FLNODS+Snode,FLNODS+Snode+2
        NSEL,A,node,,MLNODS+Snode,MLNODS+Snode+2
        NSEL,A,node,,SLNODS+Snode,SLNODS+Snode+2
        SF,All,PRES,PRES1/20                    ! LOAD AT  WHEEL
        ALLSEL,ALL
        KBC, 0                          ! Stepped or ramped loads
        TIME, .001                       ! Time at the end of 1st transient load step
        AUTOTS,ON                           ! Auto time stepping
        NSUBST,1                        ! Time step size
        OUTRES,BASIC,2                          ! Result File Output data Options
        LSWRITE,1                       ! Write load data to load step file
        ALLSEL,ALL

*DO,I,1,RUN_No,1
        ALLSEL,ALL
        !** DELETING PREVIOUS STEP FORCES
        NSEL,S,NODE,,FLNODS+Snode+I-1,FLNODS+Snode+I+1
        NSEL,A,node,,MLNODS+Snode+I-1,MLNODS+Snode+I+1
        NSEL,A,node,,SLNODS+Snode+I-1,SLNODS+Snode+I+1
        SF,All,PRES,0                           ! LOAD AT  WHEEL

        ! APPLYING CURRENT STEP FORCES
        ALLSEL,ALL
        NSEL,S,NODE,,FLNODS+Snode+I,FLNODS+Snode+I+2
        NSEL,A,node,,MLNODS+Snode+I,MLNODS+Snode+I+2
        NSEL,A,node,,SLNODS+Snode+I,SLNODS+Snode+I+2
        SF,All,PRES,PRES1                       ! LOAD AT WHEEL
        ALLSEL,ALL
        *IF,I*XSIZE,LE,INITIAL_DIST,THEN
        Time = I*TIME_1
        TIME_AF_INDIST = Time
        DIST_AF_INDIST = I*XSIZE
        I_INITIAL_END = I
        SUB_STEP = 6
        KBC,0                           ! Stepped or ramped loads
        TIME,Time                        ! Time at the end of nth transient load step
        AUTOTS,ON                           ! Auto time stepping
        NSUBST,SUB_STEP,6,2
                ! No of sub_step  in given step
        OUTRES,BASIC,2                          ! Result File Output data Options
```

```
        LSWRITE,I+1                         ! Write load data to load step file

        *ELSEIF,I*XSIZE,LE,FINIAL_DIST,THEN
        DIST = I*XSIZE-DIST_AF_INDIST
        SQ_TERM = (-2*I_Vel+SQRT(4*I_Vel*I_Vel+8*ACC*DIST))/(2*ACC)
        Time = TIME_AF_INDIST+ SQ_TERM
        I_FINIAL_END = I
        TIME_AF_FIDIST = Time
        SUB_STEP = 6
        KBC,0                           ! Stepped or ramped loads
        TIME,Time                        ! Time at the end of nth transient load step
        AUTOTS,ON                           ! Auto time stepping
        NSUBST,SUB_STEP,6,2
                ! No of sub_step  in given step
        OUTRES,BASIC,2                      ! Result File Output data Options
        LSWRITE,I+1                         ! Write load data to load step file

        *ELSE
        Time = TIME_AF_FIDIST+(I-I_FINIAL_END)*TIME_2
        SUB_STEP = 6
        KBC,0                           ! Stepped or ramped loads
        TIME,Time                        ! Time at the end of nth transient load step
        AUTOTS,ON                           ! Auto time stepping
        NSUBST,SUB_STEP,6,2
                ! No of sub_step  in given step
        OUTRES,BASIC,2                      ! Result File Output data Options
        LSWRITE,I+1                         ! Write load data to load step file
        *ENDIF

        ALLSEL,ALL
*ENDDO
CNVTOL,F,50,0.1                                         ! VALUE = 5 N , TOL
= 5 %
DSPOPTION,PARORDER,INCORE, , ,PERFORMANCE
LSSOLVE,1,RUN_No+1,1                ! initiate multiple load step solution
Finish
/EOF
```